Published OnlineFirst June 4, 2019; DOI: 10.1158/0008-5472.CAN-18-3275

Molecular Cell Biology

Cancer Research

A Model System for Studying the DNMT3A Hotspot Mutation (DNMT3A^{R882}) Demonstrates a Causal Relationship between Its Dominant-Negative Effect and Leukemogenesis

Rui Lu[1,2], Jun Wang[1,2], Zhihong Ren[1,2], Jiekai Yin[3,4], Yinsheng Wang[3,4], Ling Cai[1,5], and Gang Greg Wang[1,2]

Abstract

Mutation of DNA methyltransferase 3A at arginine 882 (DNMT3A^{R882mut}) is prevalent in hematologic cancers and disorders. Recently, DNMT3A^{R882mut} has been shown to have hypomorphic, dominant-negative, and/or gain-of-function effects on DNA methylation under different biological contexts. However, the causal role for such a multifaceted effect of DNMT3A^{R882mut} in leukemogenesis remains undetermined. Here, we report TF-1 leukemia cells as a robust system useful for modeling the DNMT3A^{R882mut}-dependent transformation and for dissecting the cause–effect relationship between multifaceted activities of DNMT3A^{R882mut} and leukemic transformation. Ectopic expression of DNMT3A^{R882mut} and not wild-type DNMT3A promoted TF-1 cell transformation characterized by cytokine-independent growth, and induces CpG hypomethylation predominantly at enhancers. This effect was dose dependent, acted synergistically with the isocitrate dehydrogenase 1 (IDH1) mutation, and resembled what was seen in human leukemia patients carrying DNMT3A^{R882mut}. The transformation- and hypomethylation-inducing capacities of DNMT3A^{R882mut} relied on a motif involved in heterodimerization, whereas its various chromatin-binding domains were dispensable. Mutation of the heterodimerization motif that interferes with DNMT3A^{R882mut} binding to endogenous wild-type DNMT proteins partially reversed the CpG hypomethylation phenotype caused by DNMT3A^{R882mut}, thus supporting a dominant-negative mechanism in cells. In mice, bromodomain inhibition repressed gene-activation events downstream of DNMT3A^{R882mut}-induced CpG hypomethylation, thereby suppressing leukemogenesis mediated by DNMT3A^{R882mut}. Collectively, this study reports a model system useful for studying DNMT3A^{R882mut}, shows a requirement of the dominant-negative effect by DNMT3A^{R882mut} for leukemogenesis, and describes an attractive strategy for the treatment of leukemias carrying DNMT3A^{R882mut}.

Significance: These findings highlight a model system to study the functional impact of a hotspot mutation of DNMT3A at R882 in leukemia.

Introduction

Aberration of the epigenomic state is commonly utilized by tumors to alter gene-expression programs and to gain growth advantage (1, 2). Sequencing of primary cancer samples has identified recurrent mutations of genes involved in epigenomic regulation (2, 3). In particular, somatic mutation of DNA methyltransferase 3A (DNMT3A^{mut}) was detected in a wide range of blood cancers including 20% to 30% of acute myeloid leukemia (AML; refs. 3–7), as well as elderly individuals with clonal hematopoiesis (8–11).

DNMT3A forms a complex with accessory cofactors, serving as one of the major *de novo* DNA methyltransferases (12–14). DNMT3A (Supplementary Fig. S1A) harbors various motifs, which include a N-terminal domain (NTD) shown to interact with transcription factors (7), a Pro–Trp–Trp–Pro (PWWP) domain shown to engage methylated histone H3 lysine 36 (H3K36me; ref. 15), an ATRX–DNMT3–DNMT3L (ADD) domain known to bind specifically to the unmodified histone H3 lysine 4 (H3K4me0; refs. 14, 16), and a C-terminal catalytic domain that methylates cytosine bases, especially those in the CpG dinucleotides (12–14). Cellular contexts such as interacting partners and chromatin states are crucial for exquisite modulation of DNMT3A's genomic targeting and enzymatic functions. For

[1]Lineberger Comprehensive Cancer Center, University of North Carolina at Chapel Hill School of Medicine, Chapel Hill, North Carolina. [2]Department of Biochemistry and Biophysics, University of North Carolina at Chapel Hill, Chapel Hill, North Carolina. [3]Environmental Toxicology Graduate Program, University of California, Riverside, California. [4]Department of Chemistry, University of California, Riverside, California. [5]Department of Genetics, University of North Carolina at Chapel Hill, Chapel Hill, North Carolina.

Note: Supplementary data for this article are available at Cancer Research Online (http://cancerres.aacrjournals.org/).

Current address for Lu: Department of Medicine, UAB Comprehensive Cancer Center, University of Alabama at Birmingham, Birmingham, Alabama; and current address for Ren, Division of Hematologic Malignancies, Johns Hopkins University School of Medicine, Baltimore, Maryland.

Corresponding Author: Gang Greg Wang, University of North Carolina at Chapel Hill, School of Medicine, Lineberger Cancer Center, 450 West Drive, CB 7295, Chapel Hill, NC 27599-7295. Phone: 919-966-5952; Fax: 919-966-9673; E-mail: greg_wang@med.unc.edu

Cancer Res 2019;79:3583–94

doi: 10.1158/0008-5472.CAN-18-3275

Published OnlineFirst June 4, 2019; DOI: 10.1158/0008-5472.CAN-18-3275

example, DNMT3A adopts an auto-inhibitory conformation due to interaction between its ADD and methyltransferase domains, and such self-inhibition is released upon engagement of ADD to histone tails with H3K4me0 (14). The methyltransferase domain, which binds DNA using specified protein motifs (12), also contains crucial interfaces for forming DNMT dimers, tetramers, and/or oligomers to regulate the methylation activities (13, 14, 17–22).

DNMT3A^{mut} is primarily heterozygous in AMLs and shows a mutational hotspot at the Arg882 residue (DNMT3A^{R882mut}), which accounts for 50% to 60% of identified DNMT3A^{mut} in AMLs (2, 3, 7, 23). Because of prevalence and clinical relevance of DNMT3A^{R882mut} in blood cancer and clonal hematopoiesis, considerable progress was made in understanding the mechanisms by which DNMT3A^{R882mut} mediates transformation. DNMT3A^{R882mut} is detected in hematopoietic stem/progenitor cells (HSPC) of apparently healthy elderly individuals, supporting its role as a preleukemic founder mutation that provides initial selective advantage of mutant HSPC clones (8–11). We and others have shown that a cooperating genetic lesion is required for DNMT3A^{R882mut} or *Dnmt3a* loss to induce fully-blown leukemias in mice (24–28). Biochemically, partial loss-of-function, dominant-negative, and gain-of-function effects have all been associated to DNMT3A^{R882mut}. First, DNMT3A^{R882mut} is a hypomorphic allele and purified DNMT3A^{R882mut} enzymes display reduced methyltransferase activity on CpG substrates *in vitro* (4, 12, 29, 30). Particularly, the structure of the DNMT3A–DNMT3L–CpG complexes was recently solved, which revealed that the residue R882 forms interactions with both DNA substrates and a so-called "Target Recognition Domain" loop, a DNMT3A motif critically involved in engaging CpG dinucleotides (12). Furthermore, the dominant-negative effect was proposed for DNMT3A^{R882mut} (29, 31). Here, DNMT3A^{R882mut} associates with wild-type DNMT3A and DNMT3B, presumably interfering with the formation, stability, DNA-engaging, and/or DNA-methylating activity of the whole complex. The combined hypomorphic and dominant-negative effects of DNMT3A^{R882mut} may explain focal CpG hypomethylation seen in leukemias harboring DNMT3A^{R882mut}. On the other hand, recent studies reported an altered substrate preference of DNMT3A^{R882mut} towards CpG sites with specific flanking sequence, which is termed as the gain-of-function effect of DNMT3A^{R882mut} (32). Theoretically, these above effects of DNMT3A^{R882mut} are not mutually exclusive, indicating that DNMT3A hotspot mutation causes redistribution of DNA methylation in the cancer genome. However, it remains elusive by what effect(s) DNMT3A^{R882mut} contributes to transformation.

This study aims to determine a causal relationship between the multifaceted effect of DNMT3A^{R882mut} and leukemic transformation. Previously, the systems reported for studying the leukemia-promoting functions of DNMT3A^{R882mut} used retrovirus-based or knock-in expression of DNMT3A^{R882mut}, often in combination with other mutations, in HSPCs (24–28), which represents a challenge to perform cause–effect relationship studies of DNMT3A^{R882mut}. We here report a leukemia cell line, TF-1 cells, as a straightforward, robust cell model for assaying the DNMT3A^{R882mut}-dependent leukemic transformation and, more importantly, for dissecting the molecular basis by which DNMT3A^{R882mut} mediates transformation. We show that enforced expression of DNMT3A^{R882mut} alone, but not DNMT3A^{WT}, is sufficient to induce TF-1 cell transformation characterized by cytokine-independent growth and arrested cell differentiation. In TF-1 cells, DNMT3A^{R882mut} induces hypomethylation of CpG sites that significantly overlap those found in primary AMLs with DNMT3A^{R882mut}. With this model system, we also demonstrated the dosage effect of DNMT3A^{R882mut} on transformation, as well as cooperativity between DNMT3A^{R882mut} and IDH1 mutation, the 2 lesions coexisting in human leukemias. Importantly, this system has allowed us to systemically analyze dependency of various functional motifs within DNMT3A^{R882mut} during transformation. Here we identified a heterodimerization domain (also known as DNMT3A's heterotetramer or FF interface; refs. 13, 18–21), and not its catalytic and chromatin-binding domains, to be essential for TF-1 cell transformation. The mutation of the heterodimerization interface interfered with interaction of DNMT3A^{R882mut} with endogenous wild-type DNMT proteins and partially reversed CpG hypomethylation caused by DNMT3A^{R882mut}, supporting a dominant-negative mechanism that underlies transformation. Finally, we found the bromodomain inhibitor suppressed the gene-activation programs associated with DNMT3A^{R882mut}-induced hypomethylation. Collectively, this study describes a model system for studying the DNMT3A^{R882mut}-related leukemogenesis, demonstrates a cause–effect relationship between the dominant-negative effect and DNMT3A^{R882mut}-mediated transformation, and provides an attractive therapeutic means for treatment of leukemias carrying DNMT3A^{R882mut}.

Materials and Methods

Cell lines

The human erythroleukemic cell line TF-1 (ATCC #CRL-2003) is cultured in the RPMI1640 medium (Invitrogen) containing 10% of FBS and 2 ng/mL of recombinant human GM-CSF (R&D Systems) as described (12). Authentication of identities of parental and derived cell lines was ensured by the Tissue Culture Facility affiliated to UNC Lineberger Comprehensive Cancer Center with the genetic signature profiling and fingerprinting analysis. Every month, a routine examination of cell lines in culture for any possible mycoplasma contamination was performed using commercially available detection kits (Lonza). Cells with less than of 10 times of passages were used in the study.

Coimmunoprecipitation

Coimmunoprecipitation was carried out as previously described (33).

DNA methylation array and data analysis

Genomic DNA was extracted using the DNeasy Blood & Tissue Kit (Qiagen), followed by bisulfite-conversion using the EZ DNA Methylation-Gold Kit (Zymo Research). DNA methylation profiling was performed by the UNC Genomics Core using the Infinium HumanMethylation450 BeadChip (lllumina) according to the manufacturer's instructions. Methylation data were then subject to background subtraction and control normalization by executing preprocessIllumina in the R "minfi" package (34). Differentially methylated CpGs were identified using dmpFinder in a categorical mode. Methylation changes were considered significant at a q-value of less than 0.05 and a β value difference of more than 0.1. Hierarchical clustering analysis, scatter plots, and density plots were generated in R using "pheatmap," and "ggplot2" packages as described previously (12).

Published OnlineFirst June 4, 2019; DOI: 10.1158/0008-5472.CAN-18-3275

Chromatin immunoprecipitation followed by deep sequencing

Chromatin immunoprecipitation sequencing (ChIP-seq) was carried out using BRD4 antibody (Sigma; HPA015055) as described previously (24, 35).

Animal models

All animal experiments were reviewed and approved by the Institutional Animal Care and Use Committee of UNC. Establishment and phenotypic analysis of murine leukemia models were performed as described previously (24, 36, 37) and *in vivo* dosing of I-BET151 carried out with a described procedure (35).

Data availability

The Genomics data produced by this study, including microarray gene expression data, ChIP-seq and methylome, have been deposited in Gene Expression Omnibus (GEO) under accession code GEO: GSE130094, GSE130634, and GSE71475. The details of experimental procedures are provided in Supplementary Materials and Methods.

Results

DNMT3A^{R882mut} induces transformation of TF-1 cells characterized by cytokine-independent growth

To delineate the molecular underpinnings of DNMT3A^{R882mut}-mediated leukemogenesis, we sought to identify a robust, straightforward cell transformation system that allows cause–effect relationship studies of DNMT3A^{R882mut}. We chose to use TF-1 cells, for this leukemia line normally relies on survival-supporting cytokines to sustain cell proliferation but displays cytokine-independent growth upon acquisition of certain leukemia-related alterations such as IDH2 or TET2 mutation (38, 39). To test whether DNMT3A^{R882mut} has transformation activities in this model, we stably expressed comparable levels of DNMT3A^{WT} or a prevalent form of DNMT3A^{R882mut}, Arg882His (DNMT3A^{R882H}), into TF-1 cells (Fig. 1A insert; Supplementary Fig. S1A and S1B). In the presence of survival cytokines, TF-1 cells with either DNMT3A form showed the same rates of proliferation (Fig. 1A); however, under cytokine-poor conditions, only TF-1 cells with DNMT3A^{R882H}, not vehicle or DNMT3A^{WT}, demonstrated robust growth (Fig. 1B). Relative to controls, TF-1 cells with DNMT3A^{R882H} also showed a mild but reproducible differentiation arrest in response to differentiation signals (Supplementary Fig. S1C and S1D). As some DNMT3A mutations found in hematologic cancer are damaging ones such as frame-shifting, we asked whether TF-1 cell transformation can be recapitulated by DNMT3A loss. Indeed, knockdown of DNMT3A by independent shRNAs, and not mock, resulted in cytokine-independent proliferation (Supplementary Fig. S1E; Fig. 1C). Similar phenotypes were observed with other DNMT3A^{R882mut} variants (Arg882Cys and Arg882Ser; Fig. 1D). Next, we ask whether such a transformation phenotype requires continuous expression of DNMT3A^{R882H}. Here, a reversible expression system, which carries a pair of LoxP sites flanking the transgene (Fig. 1E, top), was used to generate cytokine-independent TF-1 lines with DNMT3A^{R882H}. After cre-mediated deletion of DNMT3A^{R882mut} (Fig. 1E, bottom; Supplementary Fig. S1F), we found that these cells no longer sustained cytokine-independent growth (Fig. 1F). Collectively, we show that DNMT3A^{R882mut} induces cytokine-independent growth of TF-1 cells and that maintenance of this phenotype relies on continuous presence of DNMT3A^{R882mut}.

DNMT3A^{R882mut} induces a CpG hypomethylation phenotype in TF-1 cells, resembling what was seen in AML patients with DNMT3A^{R882mut}

Human AMLs carrying DNMT3A^{R882mut} exhibit focal DNA hypomethylation (29), a phenotype also observed in murine leukemias with DNMT3A^{R882mut} (24). To investigate effect of DNMT3A^{R882mut} on DNA methylation in TF-1 cells, we performed methylome profiling with Illumina Infinium HumanMethylation450 BeadChip (450K array). Out of a total of 485,512 CpG sites, we identified 6,995 (1.44%) as differentially methylated CpG probes (DMP) among TF-1 lines with DNMT3A^{R882H} relative to vector-expressing controls (Fig. 2A; Supplementary Table S1). Among the identified DMPs, almost all (6,958; 99.47%) showed hypomethylation and only 37 (0.53%) displayed hypermethylation (Fig. 2A and B). In contrast, the majority of DMPs in TF-1 cells expressing DNMT3A^{WT}, relative to control, showed the increased DNA methylation (Supplementary Fig. S2A). Similar patterns of focal CpG hypomethylation were seen with DNMT3A^{R882C} and DNMT3A^{R882S} (Supplementary Fig. S2B). To delineate the genomic feature of DNMT3A^{R882H}-associated DMPs in TF-1 cells, we related the identified DMPs to 15 chromatin modifications of K562 leukemia cells (40) and found that DNMT3A^{R882H}-associated DMPs with hypomethylation occurred preferentially at gene enhancers, and not promoters or heterochromatin (Fig. 2C). These results suggest enhancer as genomic regions predominantly affected by DNMT3A^{R882H} in TF-1 cells, which is consistent with previous findings seen in murine leukemias harboring DNMT3A^{R882H} or *Dnmt3a* knockout (24, 41, 42).

To determine clinical relevance of our above finding, we compared DNMT3A^{R882mut}-associated DMPs found in TF-1 cells to those based on the TCGA methylome studies of patients with AML (3). Here, we found a significant overlap between hypomethylated DMPs identified from TF-1 cells and human AMLs with DNMT3A^{R882mut} (Fig. 2D; Supplementary Table S1), as exemplified by DMPs at *SH3TC2*, *FOXK2*, and *GP9* (Fig. 2E). In addition, principal component analysis (PCA) of DNMT3A^{R882H}-induced hypomethylated DMPs showed that the methylation pattern of TF-1 cells with DNMT3A^{R882H} resembled patients with DNMT3A^{R882mut} more than those with DNMT3A^{WT} (Supplementary Fig. S2C). Moreover, in TF-1 lines with reversible DNMT3A^{R882H} expression (Fig. 1E and F), we found that hypomethylation at the examined region relies on continuous presence of DNMT3A^{R882H} (Fig. 2F; cre+ vs. cre−). Together, we show that DNMT3A^{R882H}-expressing TF-1 cells carry methylation alterations shared by human AMLs, lending support for using TF-1 cells as a model to study DNMT3A^{R882mut}.

DNMT3A^{R882H} and IDH mutations cooperate to promote TF-1 cell transformation

In the clinic, DNMT3A and IDH1/2 mutations frequently cooccur (3) and genetic interaction between DNMT3A^{R882H} and IDH2^{R140Q} was verified in mice (42). To query whether TF-1 cells is also suitable for studying synergy between IDH and DNMT3A mutations, we established TF-1 lines with expression of DNMT3A^{R882H}, IDH1^{R132H}, or their combination (Fig. 3A). TF-1 cells expressing either mutation showed considerable proliferation postremoval of survival cytokines; however, significantly more growth under cytokine-poor conditions was seen with cells carrying both mutations (Fig. 3B). Methylome analysis revealed that DNMT3A^{R882H} alone and IDH1^{R132H} alone predominantly

Published OnlineFirst June 4, 2019; DOI: 10.1158/0008-5472.CAN-18-3275

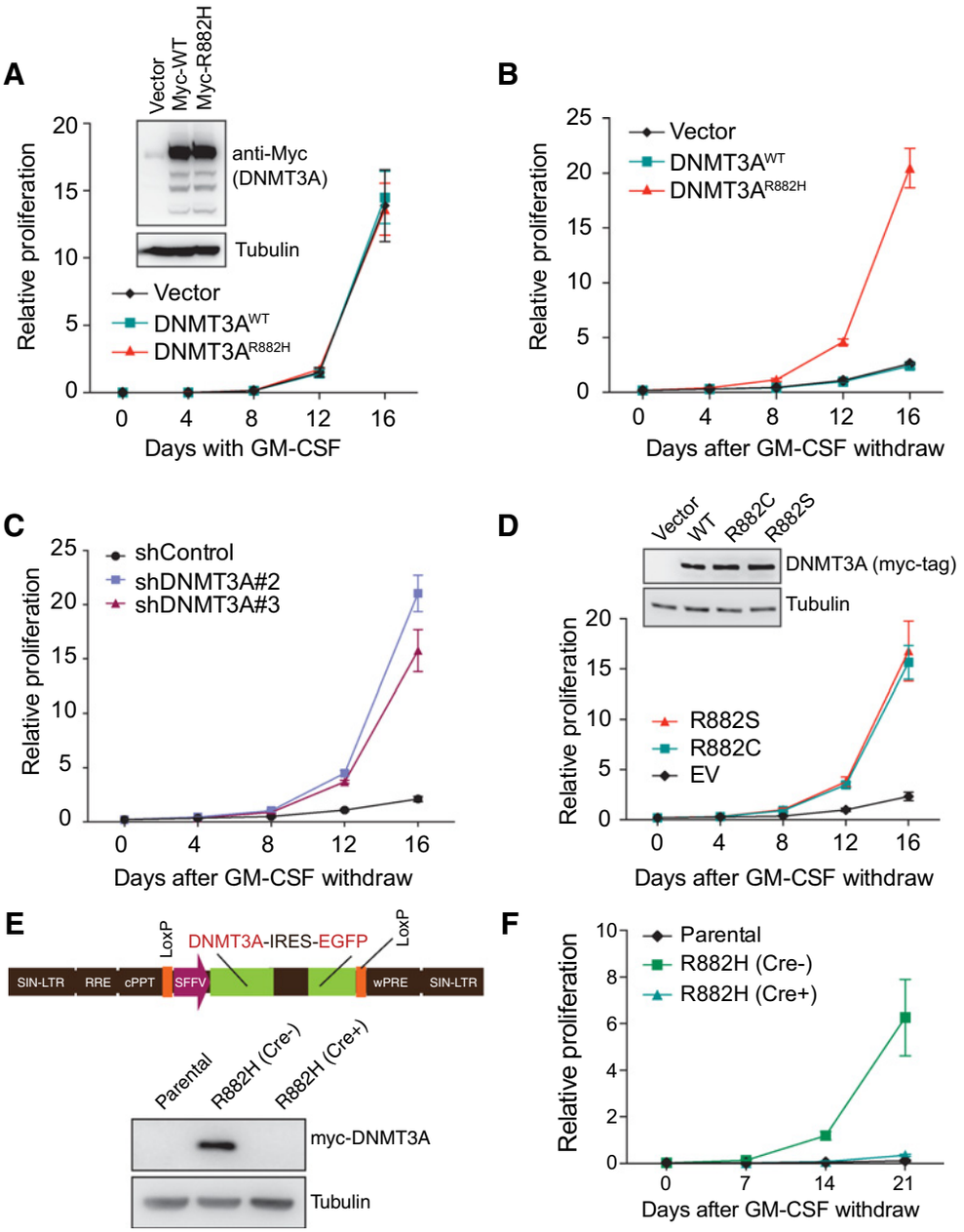

Figure 1.

R882-mutated DNMT3A (DNMT3A^{R882mut}), and not the wild-type one (DNMT3A^{WT}), induces transformation of TF-1 cells characterized by cytokine-independent growth. **A** and **B,** Proliferation of TF-1 cells with stable transduction of the indicated gene in the presence (**A**) and absence (**B**) of GM-CSF. Inset in **A**, anti-Myc immunoblotting of tagged DNMT3A. **C,** Proliferation of TF-1 cells posttransduction of shRNA vector (control) or DNMT3A-targeted shRNAs under the GM-CSF–depleted culture condition. **D,** Proliferation of TF-1 cells with stable expression of vector, DNMT3A^{WT}, or DNMT3A^{R882mut} (DNMT3A$^{R882C/S}$) upon GM-CSF removal. Inset, anti-Myc immunoblotting of tagged DNMT3A. **E,** A vector LEGO-iG2 (top) that allows the cre-mediated depletion and thus reversible expression of DNMT3A^{R882H} as verified by immunoblotting (bottom). **F,** Proliferation of the indicated TF-1 lines upon GM-CSF removal after depletion of DNMT3A^{R882H} under the cytokine-rich condition.

induced hypo- and hypermethylation, respectively (Fig. 3C), with the commonly affected sites accounting for merely nearly 5% to 10% (Fig. 3D). These suggest that DNMT3A^{R882H} and IDH1^{R132H} target different genomic regions to induce methylation changes. Moreover, a large majority of CpGs affected by either mutation alone were no longer affected in TF-1 cells with dual mutations, whereas new events of hyper- and hypomethylation at additional CpG sites were gained by these cells (Fig. 3E). This phenomenon of "epigenetic antagonism" is similar to what was seen in AMLs carrying dual mutations of DNMT3A^{R882H} and IDH2^{R140Q} (42). Together, our results support TF-1 cells as a model useful for studying synergistic effect of DNMT3A and IDH1 mutations.

Published OnlineFirst June 4, 2019; DOI: 10.1158/0008-5472.CAN-18-3275

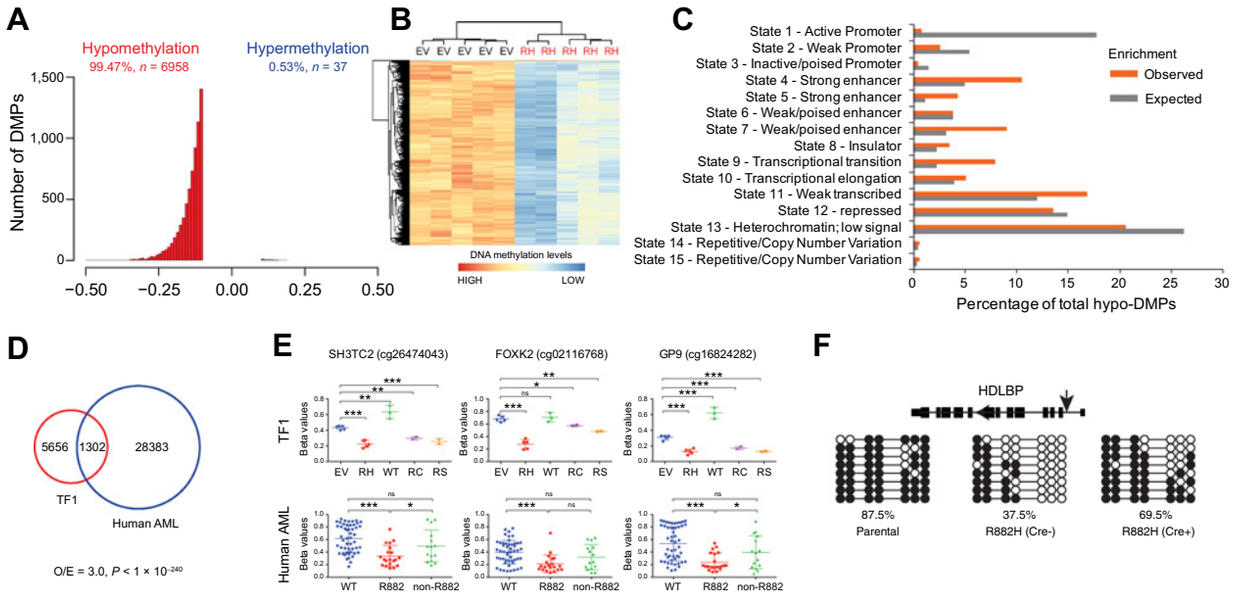

Figure 2.

DNMT3A^{R882mut} mainly induces DNA hypomethylation in TF-1 cells. **A,** Distribution of differentially methylated probes (DMP), either hypo- (left) or hyper-methylated (right), as defined in TF-1 stable cell lines with DNMT3A^{R882H}, relative to vector controls, cultured in the presence of GM-CSF. **B,** Heatmap shows relative methylation of DMPs defined in **A** among independent TF-1 lines with stable transduction of DNMT3A^{R882H} (RH; $n = 5$) or empty vector (EV; $n = 5$). **C,** Enrichment of DNMT3A^{R882H}-induced hypomethylated DMPs at genomic features annotated by the ENCODE K562 ChromHMM (40). **D,** Venn diagram shows significant overlapping between DMPs with the DNMT3A^{R882H}-induced hypomethylation in TF-1 cells and those associated with DNMT3A^{R882mut} in human AMLs (29). **E,** Methylation levels indicated by β values (y-axis) at representative DNMT3A^{R882H}-associated DMPs in the indicated TF-1 lines expressing EV, DNMT3A^{WT}, or DNMT3A^{R882mut} (RH, RC, or RS; top) or among human AMLs with DNMT3A^{WT} or DNMT3A^{mut} at the R882 or non-R822 residue (bottom). **F,** Sanger sequencing showing CpG methylation levels at the indicated site (top; black arrow) in parental TF-1 cells (left) or those transformed lines before (middle) and after depletion of DNMT3A^{R882H} (right; see also Fig. 1E and F).

Effect of DNMT3A^{R882mut} on CpG hypomethylation and TF-1 cell transformation is dosage dependent

DNMT3A^{R882mut} is believed to act as a founder mutation during leukemogenesis, and there is an age-dependent increase in incidence of clonal hematopoiesis among individuals carrying DNMT3A^{R882mut} (8, 9). These studies indicate that effect of DNMT3A^{R882mut} might be time and dose dependent, with affected epigenomic alterations accumulating during the course of disease progression. To test this hypothesis, we coexpressed DNMT3A^{R882mut} together with GFP in an internal ribosome entry site (IRES)-based coexpression system and, based on GFP sorting, we established a set of TF-1 stable lines with increasing levels of DNMT3A^{R882H}–IRES-GFP expression (Supplementary Fig. S3A). By RT-PCR and immunoblotting, we confirmed serially increased DNMT3A^{R882H} levels in cells (Fig. 4A and B). Using 450K arrays, we found a positive correlation between DNMT3A^{R882H} dosage and the total number of DMPs with induced hypomethylation (Fig. 4C), as exemplified by those at *SH3TC2* and *GP9* (Supplemental Fig. 3B). Importantly, cultivation under cytokine-poor conditions showed the cytokine-independent outgrowth also correlated with the DNMT3A^{R882H} dosage (Fig. 4D). As control, we also established TF1 lines with increasing expression of DNMT3A^{WT} (Fig. 4A and B) and found that the DNMT3A^{WT} dosages had no effect on cytokine-independent growth (Fig. 4D). These results demonstrate a dose-dependent action for DNMT3A^{R882mut} in inducing CpG hypomethylation and TF-1 cell transformation.

Effect of DNMT3A^{R882mut} on TF-1 leukemia cell transformation is independent of its catalytic function

Previously, it was shown that DNMT3A^{R882mut} is not a null mutant and shows a mildly or partially reduced methyltransferase activity as assayed *in vitro* (4, 12, 20, 29, 30). Moreover, recent studies reported that, relative to DNMT3A^{WT}, DNMT3A^{R882mut} exhibits the increased methylation activity *in vitro* towards certain CpG substrates with a specific flanking sequence, implicating a gain-of-function action (32). However, to what extent gain-of-function effect of DNMT3A^{R882mut} contributes to transformation remains undefined. First, we found that, in TF-1 cells with DNMT3A^{R882mut}, the induced hypermethylation only represents a minor event (Fig. 2A). This is reminiscent of what was observed in murine DNMT3A^{R882H}-expressing HSPCs with a more comprehensive enhanced reduced representation bisulfite sequencing (eRRBS) platform where hypomethylation accounted for 80.8% of detected changes (24). Next, we closely examined this published eRRBS dataset and focused on sites with hypermethylation and direct binding of DNMT3A^{R882H} (24). Here, we did not observe significant preference towards CpG-flanking sequences (Supplementary Fig. S4A and S4B). Next, to testify whether the enzymatic activity retained in DNMT3A^{R882mut} is essential for transformation, we introduced an enzymatic-dead mutation, P709V/C710D or E756A (12, 15), into DNMT3A^{R882H}, followed by TF-1 cell transduction (Fig. 5A). Under cytokine-poor culture conditions, neither of enzymatic-dead mutations interfered with the transforming capacity of DNMT3A^{R882H} (Fig. 5B). These observations support that the remaining catalytic

Published OnlineFirst June 4, 2019; DOI: 10.1158/0008-5472.CAN-18-3275

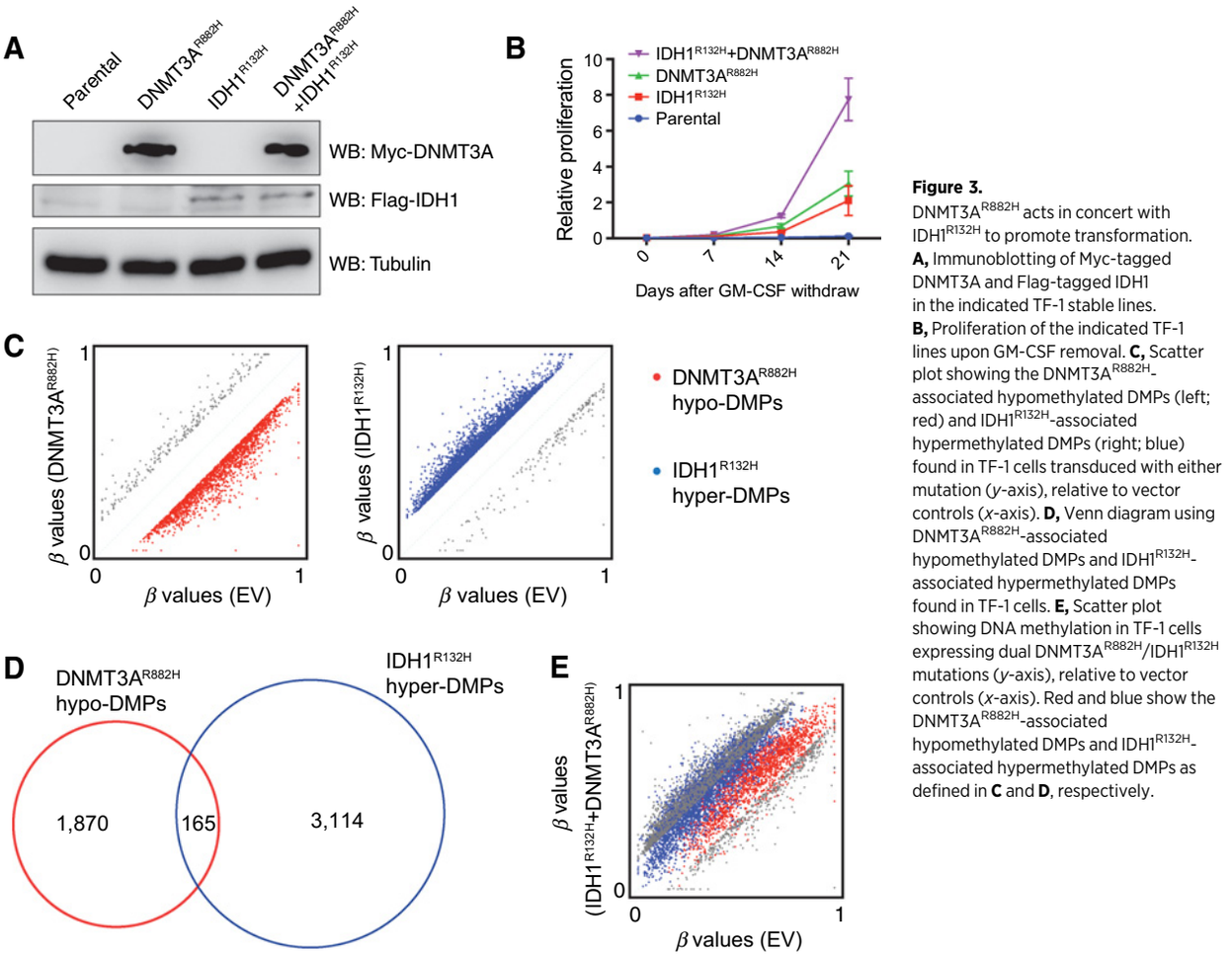

Figure 3.
DNMT3A^{R882H} acts in concert with IDH1^{R132H} to promote transformation. **A,** Immunoblotting of Myc-tagged DNMT3A and Flag-tagged IDH1 in the indicated TF-1 stable lines. **B,** Proliferation of the indicated TF-1 lines upon GM-CSF removal. **C,** Scatter plot showing the DNMT3A^{R882H}-associated hypomethylated DMPs (left; red) and IDH1^{R132H}-associated hypermethylated DMPs (right; blue) found in TF-1 cells transduced with either mutation (*y*-axis), relative to vector controls (*x*-axis). **D,** Venn diagram using DNMT3A^{R882H}-associated hypomethylated DMPs and IDH1^{R132H}-associated hypermethylated DMPs found in TF-1 cells. **E,** Scatter plot showing DNA methylation in TF-1 cells expressing dual DNMT3A^{R882H}/IDH1^{R132H} mutations (*y*-axis), relative to vector controls (*x*-axis). Red and blue show the DNMT3A^{R882H}-associated hypomethylated DMPs and IDH1^{R132H}-associated hypermethylated DMPs as defined in **C** and **D**, respectively.

activity harbored within DNMT3A^{R882mut} is not essential for transformation.

Effect of DNMT3A^{R882H} on TF-1 leukemia cell transformation relies on its heterodimerization interface and not chromatin-binding motifs

To dissect the basis underlying DNMT3A^{R882mut}-mediated transformation, we systematically mutated its functional motifs (Fig. 5C) that were known to mediate chromatin or protein–protein interactions (19). First, we found that, unlike deletion of the NTD or PWWP domains, deletion of ADD severely affected protein stability of DNMT3A^{R882H} (Fig. 5D). Thus, we also used point mutations of the motif that did not affect stability, D333A (D329A in mouse Dnmt3a) and D529A/D531A shown to disrupt the H3K36me3- and H3K4me0-binding of PWWP and ADD, respectively (Fig. 5E and F; refs. 14, 15). Relative to DNMT3A^{R882H}, all derived deletion or double mutants affecting the NTD, PWWP, or ADD domain showed comparable abilities to sustain cytokine-free proliferation in TF-1 cells (Fig. 5G and H).

DNMT3L is not expressed in AML (29) and DNMT3A may form high-order protein complexes with itself (17, 18, 20, 22, 29, 32, 43) or DNMT3B (31, 44, 45). DNMT3A^{R882mut} was proposed to act in a dominant-negative manner by "hijacking" and interfering with functions of wild-type DNMT3A/B proteins via a heterodimerization interface (29, 31). However, the causal role for such an effect in leukemic transformation has not been formally tested. To this end, we introduced into DNMT3A^{R882H} a mutation previously shown to disrupt the heterodimerization-interface-mediated interaction, i.e. F732A or Y735A (Fig. 5E; Supplementary Fig. S4C; refs. 18, 20). After transduction into TF-1 cells, the DNMT3A$^{R882H/Y735A}$ double mutant showed comparable protein stability (Fig. 5F) whereas DNMT3A$^{R882H/F732A}$ was unstable and excluded from subsequent analyses (Supplementary Fig. S4D). We found that, relative to DNMT3A^{R882H}, DNMT3A$^{R882H/Y735A}$ displayed significantly reduced abilities to sustain cytokine-free growth of TF-1 cells (Fig. 5H, orange).

To gain mechanistic insights, we further assessed interactions of DNMT3A$^{R882H/F732A}$ with endogenous DNMTs, and observed that, relative to DNMT3A^{R882H}, DNMT3A$^{R882H/Y735A}$ is defective in forming efficient interactions with wild-type DNMT3A and DNMT3B in cells (Fig. 6A), which is in agreement with *in vitro* analysis of mutations affecting this heterodimerization or FF interface (18, 20). Next, we examined methylation changes induced by the double mutant forms of DNMT3A^{R882H}. Consistent with transformation results, deletion or point mutation of PWWP and ADD did not interfere with the ability of DNMT3A^{R882H} to induce hypomethylation (Fig. 6B). In contrast,

Published OnlineFirst June 4, 2019; DOI: 10.1158/0008-5472.CAN-18-3275

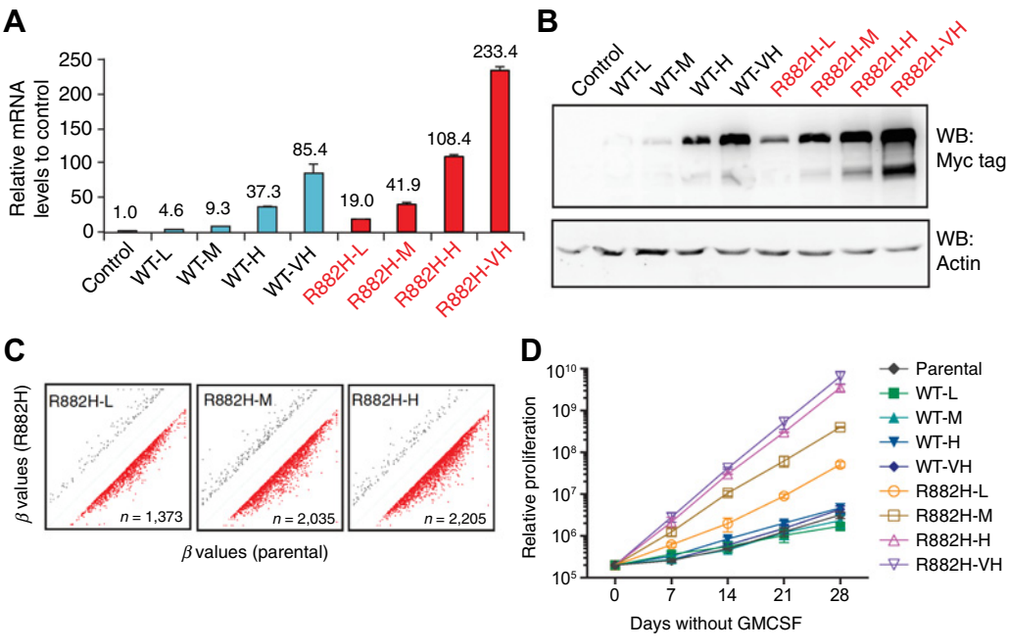

Figure 4.

DNMT3A^{R882H} promotes leukemic cell transformation and CpG hypomethylation in a dose-dependent manner. **A** and **B,** RT-qPCR (**A**) and immunoblot (**B**) validation of serially increased levels of Myc-tagged DNMT3A, either WT (blue) or R882H-mutated (red), after GFP-based sorting of TF-1 cells. Expression values shown **A** were normalized to control. Control, parental TF-1 cells. L, M, H, VH denote low, medium, high, very high, respectively. **C,** Scatter plot showing DNA methylation levels of DMPs in TF-1 lines expressing the serially increased DNMT3A^{R882H} (*y*-axis; either the L, M, or H level in expression) relative to vector controls (*x*-axis). DMPs were defined with a β value change more than 0.15 and a *P* value less than 0.05. Hypo-DMPs are marked in reds, with their numbers labeled at the bottom; hyper-DMPs are marked in gray. **D,** Proliferation of TF-1 cells expressing the indicated different levels of DNMT3A, either WT or R882H-mutated, upon cytokine removal.

much fewer of CpG sites exhibited significant hypomethylation in TF-1 cells posttransduction of DNMT3A$^{R882H/Y735A}$ (Fig. 6B).

DNA methylation is implicated in regulation of numerous cellular processes including transcription, genome stability, and mRNA splicing (46, 47). Here, we aimed to gain a glimpse of how DNMT3A^{R882H} affects gene transcription. We looked closely at LMO2, a transcription factor related to leukemogenesis (48) including AML with Dnmt3a mutation (28), for LMO2 shows consistent CpG hypomethylation in TF1 cells with DNMT3A$^{R882-mut}$ and TCGA methylome studies of patients with AML (Supplementary Fig. S5; Supplementary Table S1). By RT-qPCR, we found expression of LMO2 activated in TF-1 cells with DNMT3A^{R882H} but repressed in those with DNMT3A^{WT}, relative to control (Fig. 6C, middle); furthermore, the heterodimerization-interface-defective mutation, Y735A, significantly interfered with the LMO2-activating effect of DNMT3A^{R882H} (Fig. 6C, right).

Together, we show that disrupting heterodimerization interactions severely interferes with the ability of DNMT3A^{R882H} to induce CpG hypomethylation, LMO2 activation, and cytokine-free growth in TF-1 cells.

Bromodomain inhibition reversed gene-activation events downstream of DNMT3A^{R882H}-mediated CpG hypomethylation, providing a means for treating AMLs with DNMT3A^{R882H}

Our above observations support a causal relationship between transformation and CpG hypomethylation, which is most likely due to combined hypomorphic and dominant-negative effects by DNMT3A^{R882H}. This further indicates that targeting events downstream of the induced CpG hypomethylation represents a therapeutic strategy. Our prior study of DNMT3A^{R882H}–dependent murine AML models has revealed a marked increase of histone acetylation at gene-regulatory regions carrying DNMT3A^{R882H}–induced CpG hypomethylation (24). Histone acetylation "readers" such as BRD4 engage acetylated histones, potentiating gene activation. Using ChIP-seq performed with DNMT3A^{R882H}–dependent murine AML cells, we found H3K27ac and BRD4 bound at the DNMT3A^{R882H}–associated target signature genes that we previously defined (24), which include leukemia-related "stemness" and prosurvival oncogenes such as *Mn1*, *Mycn*, and *Bcl2* (Fig. 7A). Next, we queried whether BRD4 inhibition has therapeutic effect. We first examined sensitivity to I-BET151, a BRD4 inhibitor, using murine AML lines we previously established with dual DNMT3A^{R882H} and RAS mutations (24). A strong growth inhibition effect of I-BET151 was observed, with IC_{50} calculated at ~100 nmol/L (Fig. 7B). Importantly, transcriptome analysis showed that BRD4 blockade resulted in downregulation of DNMT3A^{R882H}–associated target signature genes (Fig. 7C and D; ref. 24). As well, gene ontology (GO) analysis showed that I-BET151 caused profound changes, including upregulation of apoptosis-related genes and downregulation of cell-cycle progression genes (Supplementary Fig. S6A). Gene set enrichment analysis (GSEA) further revealed that genes related to MYC targets, stemness, proliferation, DNA replication, and cancer-associated signatures were all suppressed by I-BET151 (Fig. 7E–G; Supplementary Fig. S6B).

Next, we evaluated *in vivo* therapeutic effect of I-BET151 on murine AMLs induced by dual DNMT3A^{R882H} and RAS^{G12D}

Published OnlineFirst June 4, 2019; DOI: 10.1158/0008-5472.CAN-18-3275

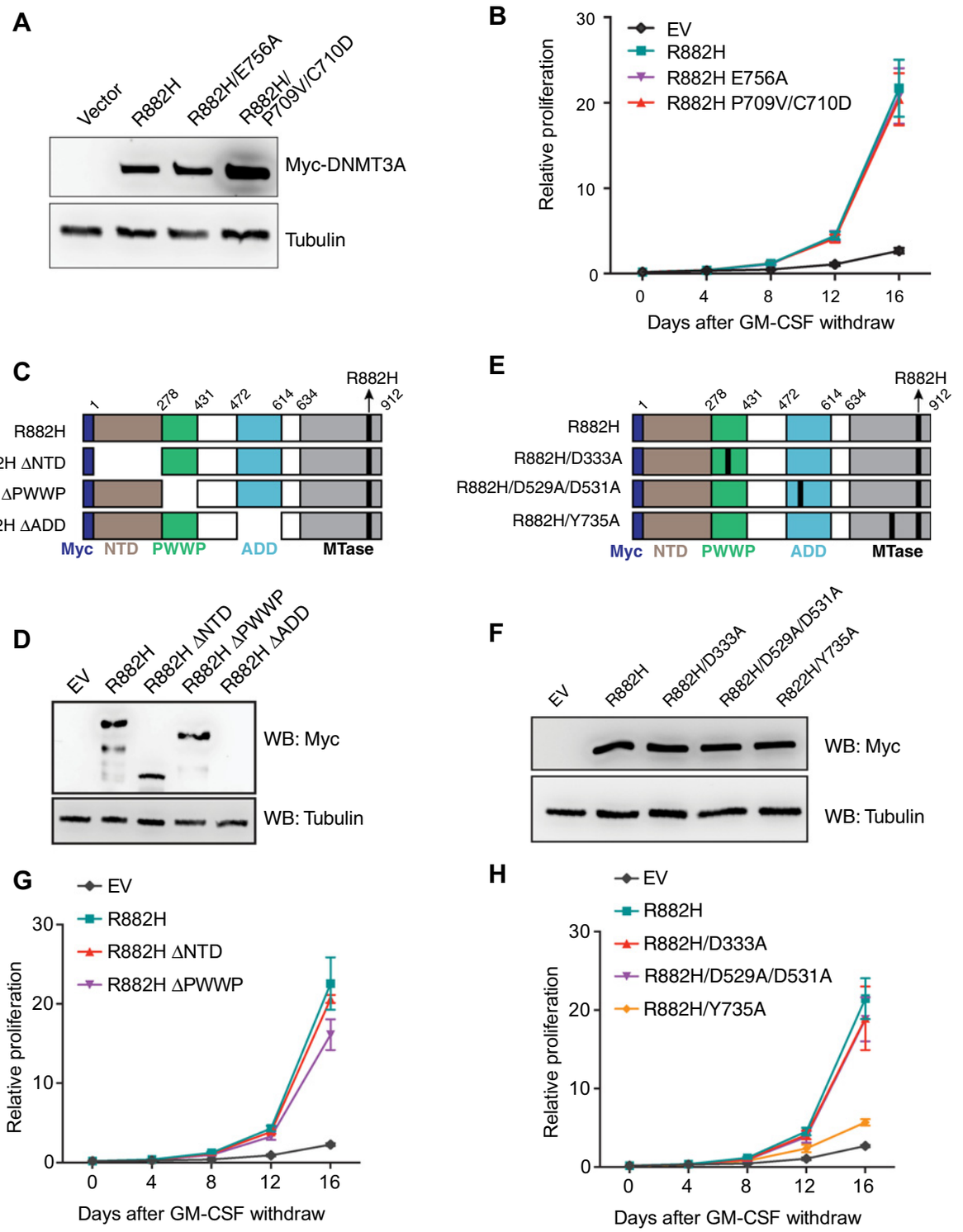

Figure 5.

Effect of DNMT3A^{R882H} on TF-1 cell transformation is independent of its catalytic function but requires its heterodimerization interface. **A,** Immunoblot showing the level of the indicated Myc-tagged DNMT3A mutant posttransduction into TF-1 cells. **B,** Proliferation of TF-1 cells expressing the indicated DNMT3A mutant upon cytokine removal. **C–F,** Schematic representation of different truncation (**C**) or point mutation (**E**) of Myc-tagged DNMT3A^{R882H}, with anti-Myc immunoblots (**D** and **F**) showing their protein levels posttransduction into TF-1 cells. EV, empty vector. **G** and **H,** Proliferation of TF-1 cells expressing the indicated truncation (**G**) or point mutant form (**H**) of DNMT3A^{R882H} upon cytokine removal.

Published OnlineFirst June 4, 2019; DOI: 10.1158/0008-5472.CAN-18-3275

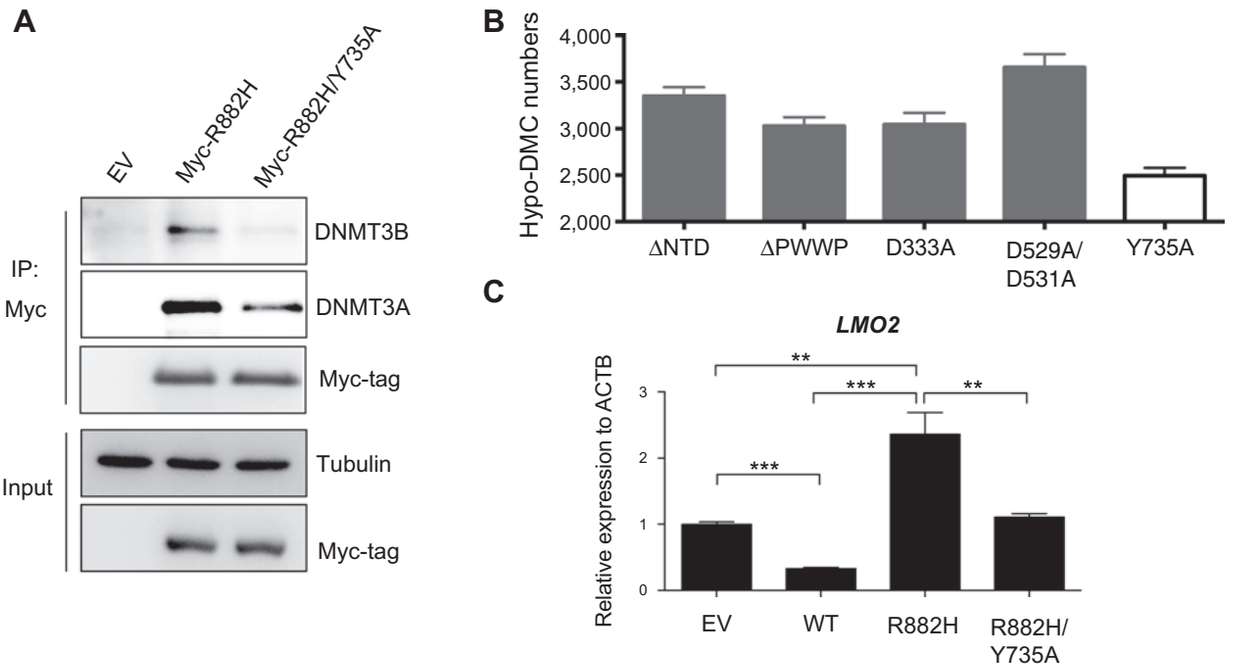

Figure 6.

CpG hypomethylation-inducing effect of DNMT3A^{R882H} requires its heterodimerization interface. **A,** Coimmunoprecipitation with anti-Myc antibodies detects interaction of the Myc-tagged DNMT3A^{R882H} (middle) or DNMT3A$^{R882H/Y735A}$ (right) with endogenous wild-type DNMT3B or DNMT3A proteins. **B,** Summary of the total number of hypomethylated DMPs induced by the indicated variant forms of DNMT3A^{R882H}, relative to vector control (as shown in Fig. 2A; with β value decrease more than 0.1). **C,** RT-qPCR detecting expression of LMO2 in TF-1 lines with stable transduction of empty vector (EV) or the indicated DNMT3A forms at day 12 post-withdrawal of GM-CSF. **, $P < 0.01$; ***, $P < 0.001$.

mutations. Compared with mock, I-BET151 treatment significantly prolonged survival of leukemic mice (Fig. 7H). Compared with mock, I-BET151 treatment also significantly delayed development of AML phenotypes such as splenomegaly, elevated counts of white blood cells and reduce counts of red blood cells (Fig. 7I and J; Supplementary Fig. S4C). Following I-BET151 treatment, less AML blasts were also observed in the bone marrow (Fig. 7J, bottom). Given that I-BET151 inhibits the DNMT3A^{R882H}-related gene-expression programs, we next ask whether inhibition of RAS signaling has additional therapeutic effect in this model. To this end, we used trametinib, an FDA-approved inhibitor of MEK (49). Indeed, while dosing with trametinib or I-BET151 alone considerably delayed AML progression as measured by animal survival and bioluminescence imaging, their combinational treatment had more significant AML-inhibitory effect *in vivo* (Fig. 7K and L).

Collectively, bromodomain inhibition not only represses gene-expression programs related to DNMT3A^{R882H}-induced hypomethylation but, importantly, suppresses development of the DNMT3A^{R882H}-related murine AMLs *in vivo*, either alone or in combination with MEK inhibitors.

Discussion

DNMT3A^{mut} is prevalent in patients with hematologic malignancies and disorders. It is proposed that DNMT3A^{mut} acts as a founder mutation shaping the course of leukemia evolution and progression. The literature has documented that DNMT3A^{R882mut} has hypomorphic, dominant-negative, and/or gain-of-function effects under different biological contexts. However, it remains undefined by what effects DNMT3A^{R882mut} mediates leukemogenesis. We started the investigations first by reporting TF1 cells as a robust system useful for studying DNMT3A^{mut}-related leukemic phenotypes, which then allowed us to next examine activities underlying DNMT3A^{R882mut}-induced transformation. Based on the mechanistic studies, we further show that BRD4 inhibition reverses gene-expression programs downstream of disease-relevant effect of DNMT3A^{R882mut}, thus suggesting a potential means of therapeutics.

Compared with the previously described *in vivo* and primary cell systems for studying DNMT3A^{R882mut} (24–28), TF-1 cells is straightforward and suitable for cause–effect relationship studies to delineate the role for multifaceted effects of DNMT3A^{R882mut} during leukemic transformation. Via a systematic interrogation of various motifs in DNMT3A^{R882mut} with this system, we show that the transformation-promoting function of DNMT3A^{R882mut} is independent of its residual catalytic activity (as assayed by double mutants carrying an enzyme-dead mutation), suggesting that CpG methylation gains at certain specific sequence contexts, as proposed in a gain-of-function model (32), is unlikely to contribute to leukemogenesis. In contrast, mutating a heterodimerization interface not only interfered with physical associations of DNMT3A^{R882mut} to endogenous wild-type DNMT3A/B proteins but also largely abolished the ability of DNMT3A^{R882mut} in inducing CpG hypomethylation and TF-1 cell transformation. These findings support a causal relationship between the dominant-negative effect of DNMT3A^{R882mut} and

Published OnlineFirst June 4, 2019; DOI: 10.1158/0008-5472.CAN-18-3275

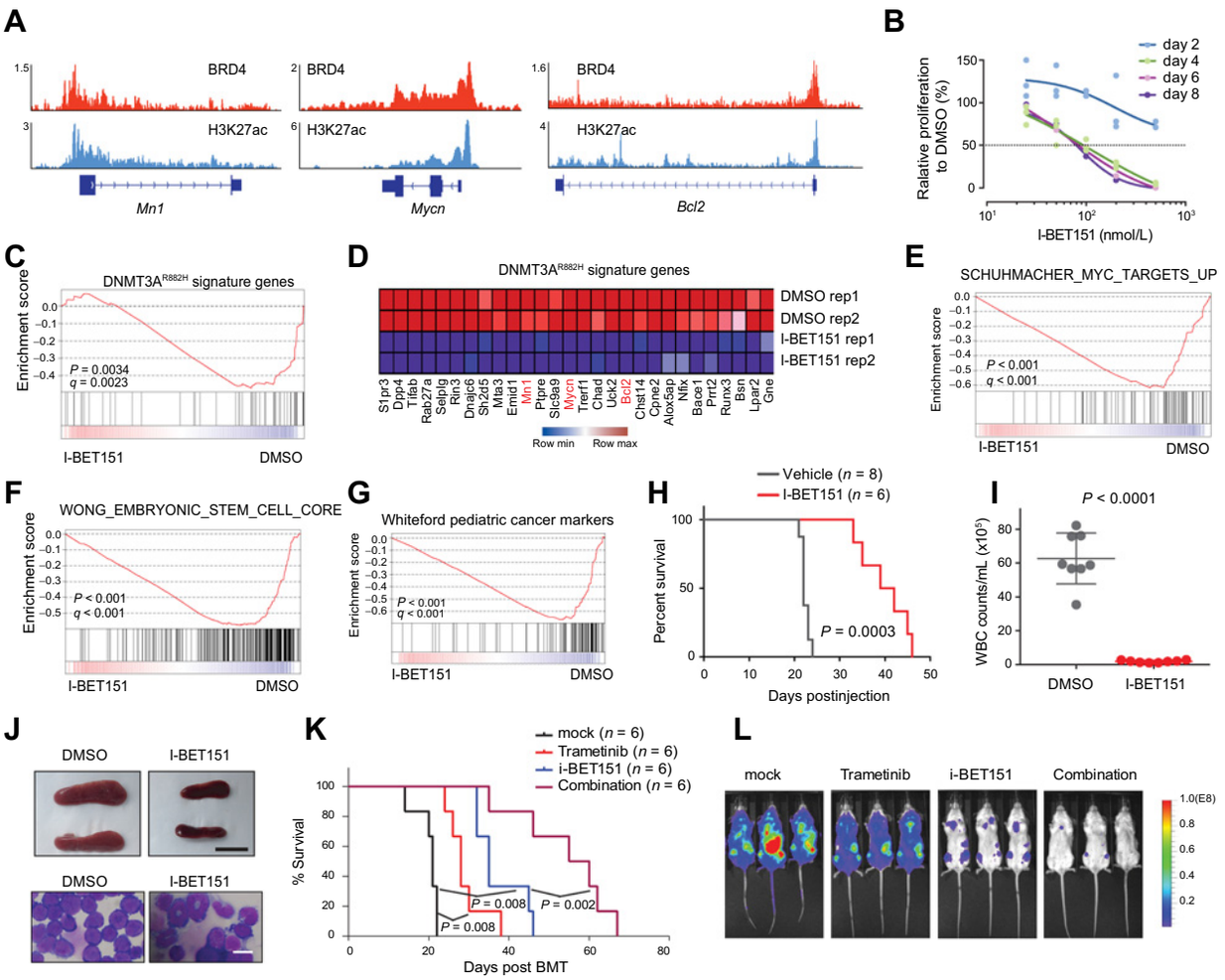

Figure 7.

BRD4 blockade is efficient in treatment of murine AML established by combinational DNMT3A^{R882H} and NRAS^{G12D} mutations. **A,** IGV track views of BRD4 and H3K27ac ChIP-seq signals at the indicated gene in murine AML cells established by coexpressed DNMT3A^{R882H} and NRAS^{G12D} (termed as murine DNMT3A^{R882H}/NRAS^{G12D} AML lines; ref. 24). **B,** Relative proliferation of the DNMT3A^{R882H}/NRAS^{G12D} AML lines posttreatment with I-BET151 relative to mock. Dashed line, IC_{50}. **C,** GSEA showing that the DNMT3A signature genes were repressed by I-BET151. Mouse_Gene_2.0_ST arrays were performed using the DNMT3A^{R882H}/NRAS^{G12D} AML cells treated with either DMSO or 100 nmol/L I-BET151 for 24 hours. **D,** Heatmap showing the most repressed DNMT3A^{R882H} signature genes by BRD4 inhibitors. Rep, replicate. **E–G,** GSEA shows downregulation of the indicated gene sets related to MYC targets (**E**), stem cell (**F**), or pediatric cancer markers (**G**) posttreatment with I-BET151. **H,** Survival of mice transplanted with the DNMT3A^{R882H}/NRAS^{G12D} AML cells and then treated with either vehicle ($n = 8$) or I-BET151 ($n = 6$; 50 mg/kg daily for 10 days). Significance was tested by log-rank test. **I** and **J,** White blood cell counts (**I**), representative images of spleens (**J**, top; scale bar, 1 cm) and Wright–Giemsa staining of bone marrow cells (**J**, bottom; scale bar, 10 μm) from mice transplanted with the DNMT3A^{R882H}/NRAS^{G12D} AML cells and treated with either vehicle or I-BET151 for 10 days. **K** and **L,** Kaplan–Meier survival curve (**K**) and representative bioluminescent images (at day 20; **L**) of mice transplanted with DNMT3A^{R882H}/NRAS^{G12D} AML cells and treated with either vehicle, trametinib (1 mg/kg daily for 10 days) , or I-BET151 alone (50 mg/kg daily for 10 days), or their combination. Significance was tested by log-rank test.

transformation. Furthermore, purified DNMT3A^{R882mut} enzymes were known to be hypomorphic (4, 12, 20, 29, 30); recent structural studies further showed that R882 forms interactions with both DNA substrates and a so-called "Target Recognition Domain" loop, which indicated its role in substrate binding and/or enzymatic functions (12). Our results thus support that combined hypomorphic and dominant-negative effects of DNMT3A^{R882mut} lead to CpG methylation decrease/loss, which is most likely to contribute to leukemogenesis. In agreement, CpG hypomethylation and not hypermethylation was detected as a major event in TF-1 cells and murine AML models carrying DNMT3A^{R882mut} (12, 24). Despite advances, exact molecular mechanism by DNMT3A^{R882mut} induces CpG hypomethylation in cells remains to be fully understood. As well, because blood cells do not express DNMT3L (29), investigation of leukemia-related DNMT3A^{mut} requires using physiologically relevant contexts such as homo-tetramers or oligomers of DNMT3A (18, 21) or complexes of DNMT3A with DNMT3B (31, 44, 45) or other putative partners.

Additionally, TF-1 cells act as a system useful for modeling various other biological effects of DNMT3A^{mut}. First, CpG hypomethylations induced by DNMT3A^{R882mut} in TF-1 cells resemble

Published OnlineFirst June 4, 2019; DOI: 10.1158/0008-5472.CAN-18-3275

those seen in leukemia patients with DNMT3A^{R882mut}, suggesting a clinical relevance of findings from this model. Furthermore, there is a dose-dependent effect by DNMT3A^{R882mut} on CpG hypomethylation and transformation (cytokine-free proliferation) in TF-1 cells, which provides an explanation for age-related increase in incidence of clonal hematopoiesis seen among elderly individuals. We observed synergy between DNMT3A^{R882mut} and IDH1 mutation in TF-1 cells, as well as a phenomenon of "epigenetic antagonism" that resembles what was seen in human AML cells carrying dual DNMT3A^{R882H} and IDH2 mutations (42). Future investigation, however, is warranted to delineate interplays between DNMT3A^{R882mut} and coexisting IDH mutations for inducing epigenomic alterations in both DNA methylation (including 5mC and 5hmC) and histone modifications. Finally, missense mutations at non-R882 residues account for nearly 40% to 50% of DNMT3A^{mut} in blood cancer and disorders. Considering many mutant forms for such a non-R882 category of DNMT3A^{mut}, TF-1 cells shall provide a simple yet robust system for studying their biological effects as shown recently with several DNMT3A^{mut} known to affect DNMT3A's DNA binding (12). Together, TF-1 cells represent a straightforward, robust, and disease-relevant model system for investigating numerous unsolved issues relating DNMT3A^{mut}.

This study not only demonstrated a requirement for the dominant-negative effect of DNMT3A^{R882mut} (most likely to act in concert with a hypomorphic nature of DNMT3A^{R882mut}) during leukemic transformation but also explored potential therapeutics. For the latter, our mechanistic studies suggest that intervention shall be developed for targeting events associated with DNMT3A^{R882mut}-induced CpG hypomethylation. Here, we first used a transgene-reversible system to show that DNMT3A^{R882mut}-induced TF-1 cell transformation relies on its continuous expression; as well, we find CpG hypomethylation correlated to transcriptional activation of LMO2, a leukemia-related oncogene, thereby providing a glimpse of how induced CpG hypomethylation influences gene expression in TF-1 cells. It is consistent to previous reports showing that sites with DNMT3A^{R882mut}-induced CpG hypomethylation are enriched in *cis*-regulatory elements such as enhancers and display increased histone acetylation, which then recruits "reader" protein complexes to potentiate gene activation (24, 50). Besides DOT1L complexes (24, 50), we here show that BRD4, another histone acetylation "reader," also binds to DNMT3A^{R882H}-associated gene targets (notably *Mn1*, *Mycn*, and *Bcl2*) in murine AMLs and that pharmacologic inhibition of BRD4 suppressed activation of DNMT3A^{R882H}-related gene signatures. BRD4 inhibitors efficiently suppressed *in vitro* and *in vivo* growth of murine AMLs carrying dual DNMT3A^{R882mut} and RAS mutations. Note that DNA methylation potentially regulates numerous biological processes including gene transcription, genome stability, chromatin architecture and looping, mRNA splicing, and silencing of repetitive DNA elements (46, 47). Determination of putative effects of DNMT3A^{R882H}-related CpG hypomethylation on these crucial processes requires future investigation.

Disclosure of Potential Conflicts of Interest

No potential conflicts of interest were disclosed.

Authors' Contributions

Conception and design: R. Lu, G.G. Wang
Development of methodology: R. Lu, J. Yin, Y. Wang, G.G. Wang
Acquisition of data (provided animals, acquired and managed patients, provided facilities, etc.): R. Lu, J. Wang, Z. Ren, J. Yin, Y. Wang, L. Cai, G.G. Wang
Analysis and interpretation of data (e.g., statistical analysis, biostatistics, computational analysis): R. Lu, J. Wang, Z. Ren, J. Yin, Y. Wang, G.G. Wang
Writing, review, and/or revision of the manuscript: R. Lu, G.G. Wang
Administrative, technical, or material support (i.e., reporting or organizing data, constructing databases): R. Lu, Z. Ren, Y. Wang, L. Cai, G.G. Wang
Study supervision: Y. Wang, G.G. Wang

Acknowledgments

We thank UNC's Genomics Core, Animal Studies Core, Flow Core, and HTSF core for their support of this work and the Wang lab for discussions. We are grateful for the help of Drs. Q. Zhang, J.A. Losman, and Y. Xiong in providing reagents and cells used in the study. This work was supported by NIH grants (R01-CA215284, R01-CA218600, and R01-CA211336 to G.G. Wang), a Kimmel Scholar Award (to G.G. Wang), a US Army/DoD Career Development Award (W81XWH-14-1-0232 to G.G. Wang), and grants of Concern Foundation for Cancer Research (to G.G. Wang), Gabrielle's Angel Foundation for Cancer Research (to G.G. Wang), Gilead Sciences Research Scholars Program (to G.G. Wang), and When Everyone Survives (WES) Leukemia Research Foundation (to G.G. Wang). UNC Core is supported in part by the North Carolina Biotech Center Institutional Support Grant 2012-IDG-1006 and the UNC Cancer Center Core Support Grant P30-CA016086. R. Lu and Z. Ren are supported by a Lymphoma Research Foundation postdoc fellowship and DoD Career Development Award nested postdoc fellowship (W81XWH-14-1-0232), respectively. G.G. Wang is an American Society of Hematology (ASH) Scholar in basic research, an American Cancer Society (ACS) Research Scholar, and a Leukemia & Lymphoma Society (LLS) Scholar.

The costs of publication of this article were defrayed in part by the payment of page charges. This article must therefore be hereby marked *advertisement* in accordance with 18 U.S.C. Section 1734 solely to indicate this fact.

Received October 17, 2018; revised April 3, 2019; accepted May 29, 2019; published first June 4, 2019.

References

1. Chi P, Allis CD, Wang GG. Covalent histone modifications–miswritten, misinterpreted and mis-erased in human cancers. Nat Rev Cancer 2010;10:457–69.
2. Shih AH, Abdel-Wahab O, Patel JP, Levine RL. The role of mutations in epigenetic regulators in myeloid malignancies. Nat Rev Cancer 2012;12:599–612.
3. Cancer Genome Atlas Research N, Ley TJ, Miller C, Ding L, Raphael BJ, Mungall AJ, et al. Genomic and epigenomic landscapes of adult de novo acute myeloid leukemia. N Engl J Med 2013;368:2059–74.
4. Yan XJ, Xu J, Gu ZH, Pan CM, Lu G, Shen Y, et al. Exome sequencing identifies somatic mutations of DNA methyltransferase gene DNMT3A in acute monocytic leukemia. Nat Genet 2011;43:309–15.
5. Ley TJ, Ding L, Walter MJ, McLellan MD, Lamprecht T, Larson DE, et al. DNMT3A mutations in acute myeloid leukemia. N Engl J Med 2010;363:2424–33.
6. Patel JP, Gonen M, Figueroa ME, Fernandez H, Sun Z, Racevskis J, et al. Prognostic relevance of integrated genetic profiling in acute myeloid leukemia. N Engl J Med 2012;366:1079–89.
7. Yang L, Rau R, Goodell MA. DNMT3A in haematological malignancies. Nat Rev Cancer 2015;15:152–65.
8. Genovese G, Kahler AK, Handsaker RE, Lindberg J, Rose SA, Bakhoum SF, et al. Clonal hematopoiesis and blood-cancer risk inferred from blood DNA sequence. N Engl J Med 2014;371:2477–87.

9. Jaiswal S, Fontanillas P, Flannick J, Manning A, Grauman PV, Mar BG, et al. Age-related clonal hematopoiesis associated with adverse outcomes. N Engl J Med 2014;371:2488–98.
10. Koeffler HP, Leong G. Preleukemia: one name, many meanings. Leukemia 2017;31:534–42.
11. Ganguly BB, Kadam NN. Mutations of myelodysplastic syndromes (MDS): An update. Mutat Res Rev Mutat Res 2016;769:47–62.
12. Zhang ZM, Lu R, Wang P, Yu Y, Chen D, Gao L, et al. Structural basis for DNMT3A-mediated de novo DNA methylation. Nature 2018;554:387–91.
13. Jia D, Jurkowska RZ, Zhang X, Jeltsch A, Cheng X. Structure of Dnmt3a bound to Dnmt3L suggests a model for de novo DNA methylation. Nature 2007;449:248–51.
14. Guo X, Wang L, Li J, Ding Z, Xiao J, Yin X, et al. Structural insight into autoinhibition and histone H3-induced activation of DNMT3A. Nature 2015;517:640–4.
15. Dhayalan A, Rajavelu A, Rathert P, Tamas R, Jurkowska RZ, Ragozin S, et al. The Dnmt3a PWWP domain reads histone 3 lysine 36 trimethylation and guides DNA methylation. J Biol Chem 2010;285:26114–20.
16. Noh KM, Wang H, Kim HR, Wenderski W, Fang F, Li CH, et al. Engineering of a histone-recognition domain in Dnmt3a alters the epigenetic landscape and phenotypic features of mouse ESCs. Mol Cell 2015;59:89–103.
17. Jeltsch A, Jurkowska RZ. Multimerization of the dnmt3a DNA methyltransferase and its functional implications. Prog Mol Biol Transl Sci 2013; 117:445–64.
18. Holz-Schietinger C, Matje DM, Harrison MF, Reich NO. Oligomerization of DNMT3A controls the mechanism of de novo DNA methylation. J Biol Chem 2011;286:41479–88.
19. Ren W, Gao L, Song J. Structural basis of DNMT1 and DNMT3A-mediated DNA methylation. Genes (Basel) 2018;9. doi: 10.3390/genes9120620.
20. Emperle M, Dukatz M, Kunert S, Holzer K, Rajavelu A, Jurkowska RZ, et al. The DNMT3A R882H mutation does not cause dominant negative effects in purified mixed DNMT3A/R882H complexes. Sci Rep 2018;8:13242.
21. Jurkowska RZ, Rajavelu A, Anspach N, Urbanke C, Jankevicius G, Ragozin S, et al. Oligomerization and binding of the Dnmt3a DNA methyltransferase to parallel DNA molecules: heterochromatic localization and role of Dnmt3L. J Biol Chem 2011;286:24200–7.
22. Kareta MS, Botello ZM, Ennis JJ, Chou C, Chedin F. Reconstitution and mechanism of the stimulation of de novo methylation by human DNMT3L. J Biol Chem 2006;281:25893–902.
23. Brunetti L, Gundry MC, Goodell MA. DNMT3A in leukemia. Cold Spring Harb Perspect Med 2017;7. doi: 10.1101/cshperspect.a030320.
24. Lu R, Wang P, Parton T, Zhou Y, Chrysovergis K, Rockowitz S, et al. Epigenetic Perturbations by Arg882-Mutated DNMT3A potentiate aberrant stem cell gene-expression program and acute leukemia development. Cancer Cell 2016;30:92–107.
25. Guryanova OA, Shank K, Spitzer B, Luciani L, Koche RP, Garrett-Bakelman FE, et al. DNMT3A mutations promote anthracycline resistance in acute myeloid leukemia via impaired nucleosome remodeling. Nat Med 2016; 22:1488–95.
26. Meyer SE, Qin T, Muench DE, Masuda K, Venkatasubramanian M, Orr E, et al. DNMT3A haploinsufficiency transforms FLT3ITD myeloproliferative disease into a rapid, spontaneous, and fully penetrant acute myeloid leukemia. Cancer Discov 2016;6:501–15.
27. Chang YI, You X, Kong G, Ranheim EA, Wang J, Du J, et al. Loss of Dnmt3a and endogenous Kras(G12D/+) cooperate to regulate hematopoietic stem and progenitor cell functions in leukemogenesis. Leukemia 2015;29: 1847–56.
28. Yang L, Rodriguez B, Mayle A, Park HJ, Lin X, Luo M, et al. DNMT3A loss drives enhancer hypomethylation in FLT3-ITD-associated leukemias. Cancer Cell 2016;29:922–34.
29. Russler-Germain DA, Spencer DH, Young MA, Lamprecht TL, Miller CA, Fulton R, et al. The R882H DNMT3A mutation associated with AML dominantly inhibits wild-type DNMT3A by blocking its ability to form active tetramers. Cancer Cell 2014;25:442–54.
30. Holz-Schietinger C, Matje DM, Reich NO. Mutations in DNA methyltransferase (DNMT3A) observed in acute myeloid leukemia patients disrupt processive methylation. J Biol Chem 2012;287:30941–51.
31. Kim SJ, Zhao H, Hardikar S, Singh AK, Goodell MA, Chen T. A DNMT3A mutation common in AML exhibits dominant-negative effects in murine ES cells. Blood 2013;122:4086–9.
32. Emperle M, Rajavelu A, Kunert S, Arimondo PB, Reinhardt R, Jurkowska RZ, et al. The DNMT3A R882H mutant displays altered flanking sequence preferences. Nucleic Acids Res 2018;46:3130–39.
33. Cai L, Rothbart SB, Lu R, Xu B, Chen WY, Tripathy A, et al. An H3K36 methylation-engaging Tudor motif of polycomb-like proteins mediates PRC2 complex targeting. Mol Cell 2013;49:571–82.
34. Aryee MJ, Jaffe AE, Corrada-Bravo H, Ladd-Acosta C, Feinberg AP, Hansen KD, et al. Minfi: a flexible and comprehensive Bioconductor package for the analysis of Infinium DNA methylation microarrays. Bioinformatics 2014; 30:1363–9.
35. Cai L, Tsai YH, Wang P, Wang J, Li D, Fan H, et al. ZFX mediates non-canonical oncogenic functions of the androgen receptor splice variant 7 in castrate-resistant prostate cancer. Mol Cell 2018;72:341–54.
36. Xu B, On DM, Ma A, Parton T, Konze KD, Pattenden SG, et al. Selective inhibition of EZH2 and EZH1 enzymatic activity by a small molecule suppresses MLL-rearranged leukemia. Blood 2015;125:346–57.
37. Wang GG, Cai L, Pasillas MP, Kamps MP. NUP98-NSD1 links H3K36 methylation to Hox-A gene activation and leukaemogenesis. Nat Cell Biol 2007;9:804–12.
38. Losman JA, Looper RE, Koivunen P, Lee S, Schneider RK, McMahon C, et al. (R)-2-hydroxyglutarate is sufficient to promote leukemogenesis and its effects are reversible. Science 2013;339:1621–5.
39. Kernytsky A, Wang F, Hansen E, Schalm S, Straley K, Gliser C, et al. IDH2 mutation-induced histone and DNA hypermethylation is progressively reversed by small-molecule inhibition. Blood 2015;125:296–303.
40. Ernst J, Kheradpour P, Mikkelsen TS, Shoresh N, Ward LD, Epstein CB, et al. Mapping and analysis of chromatin state dynamics in nine human cell types. Nature 2011;473:43–9.
41. Yang L, Rodriguez B, Mayle A, Park HJ, Lin X, Luo M, et al. DNMT3A loss drives enhancer hypomethylation in FLT3-ITD-associated leukemias. Cancer Cell 2016;30:363–65.
42. Glass JL, Hassane D, Wouters BJ, Kunimoto H, Avellino R, Garrett-Bakelman FE, et al. Epigenetic identity in AML depends on disruption of nonpromoter regulatory elements and is affected by antagonistic effects of mutations in epigenetic modifiers. Cancer Discov 2017;7: 868–83.
43. Holz-Schietinger C, Reich NO.The inherent processivity of the human de novo methyltransferase 3A (DNMT3A) is enhanced by DNMT3L. J Biol Chem 2010;285:29091–100.
44. Duymich CE, Charlet J, Yang X, Jones PA, Liang G. DNMT3B isoforms without catalytic activity stimulate gene body methylation as accessory proteins in somatic cells. Nat Commun 2016;7:11453.
45. Gordon CA, Hartono SR, Chedin F. Inactive DNMT3B splice variants modulate de novo DNA methylation. PLoS One 2013;8:e69486.
46. Jones PA. Functions of DNA methylation: islands, start sites, gene bodies and beyond. Nat Rev Genet 2012;13:484–92.
47. Lev Maor G, Yearim A, Ast G. The alternative role of DNA methylation in splicing regulation. Trends Genet 2015;31:274–80.
48. El Omari K, Hoosdally SJ, Tuladhar K, Karia D, Vyas P, Patient R, et al. Structure of the leukemia oncogene LMO2: implications for the assembly of a hematopoietic transcription factor complex. Blood 2011;117: 2146–56.
49. Burgess MR, Hwang E, Firestone AJ, Huang T, Xu J, Zuber J, et al. Preclinical efficacy of MEK inhibition in Nras-mutant AML. Blood 2014;124: 3947–55.
50. Rau RE, Rodriguez BA, Luo M, Jeong M, Rosen A, Rogers JH, et al. DOT1L as a therapeutic target for the treatment of DNMT3A-mutant acute myeloid leukemia. Blood 2016;128:971–81.

Cancer Research
The Journal of Cancer Research (1916–1930) | The American Journal of Cancer (1931–1940)

AACR American Association for Cancer Research

A Model System for Studying the DNMT3A Hotspot Mutation (DNMT3A ^{R882}) Demonstrates a Causal Relationship between Its Dominant-Negative Effect and Leukemogenesis

Rui Lu, Jun Wang, Zhihong Ren, et al.

Cancer Res 2019;79:3583-3594. Published OnlineFirst June 4, 2019.

Supplemental Figure 1

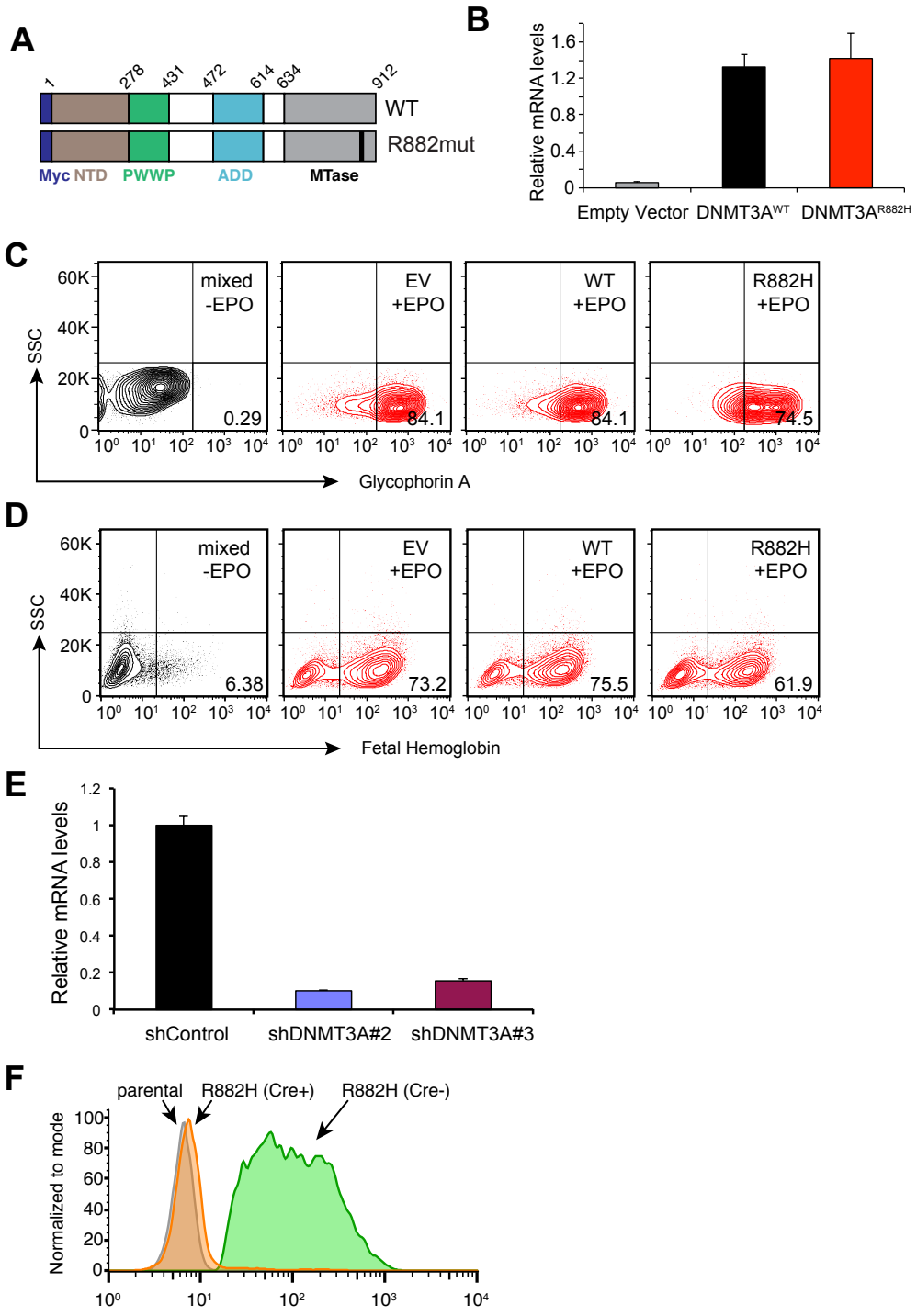

Supplemental Figure 2

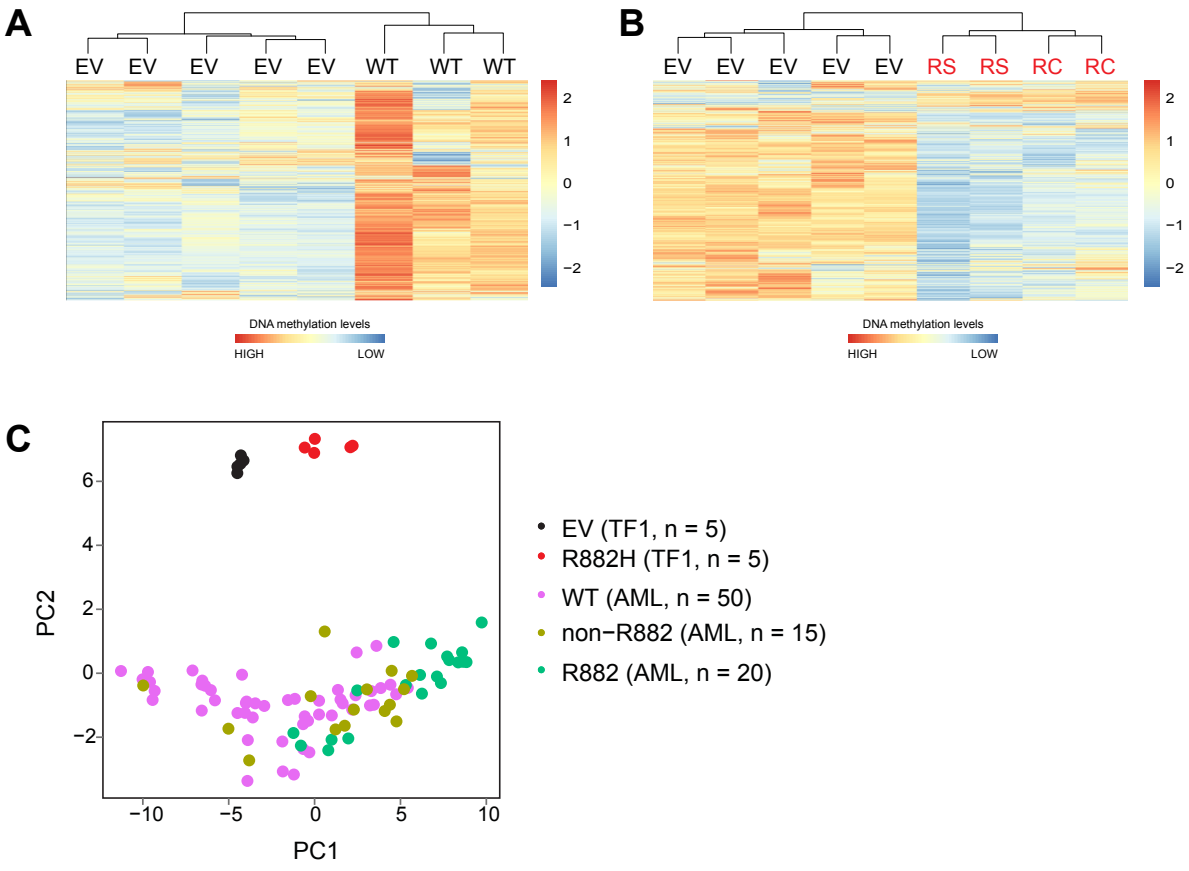

Supplemental Figure 3

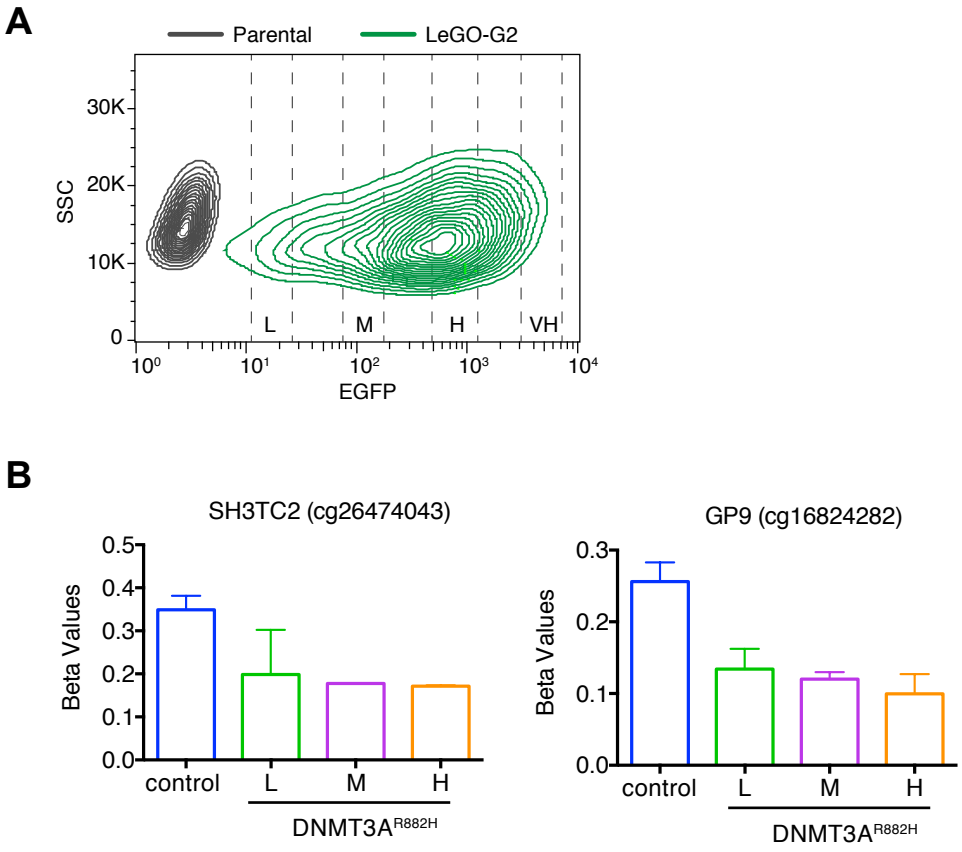

Supplementary Figure 4

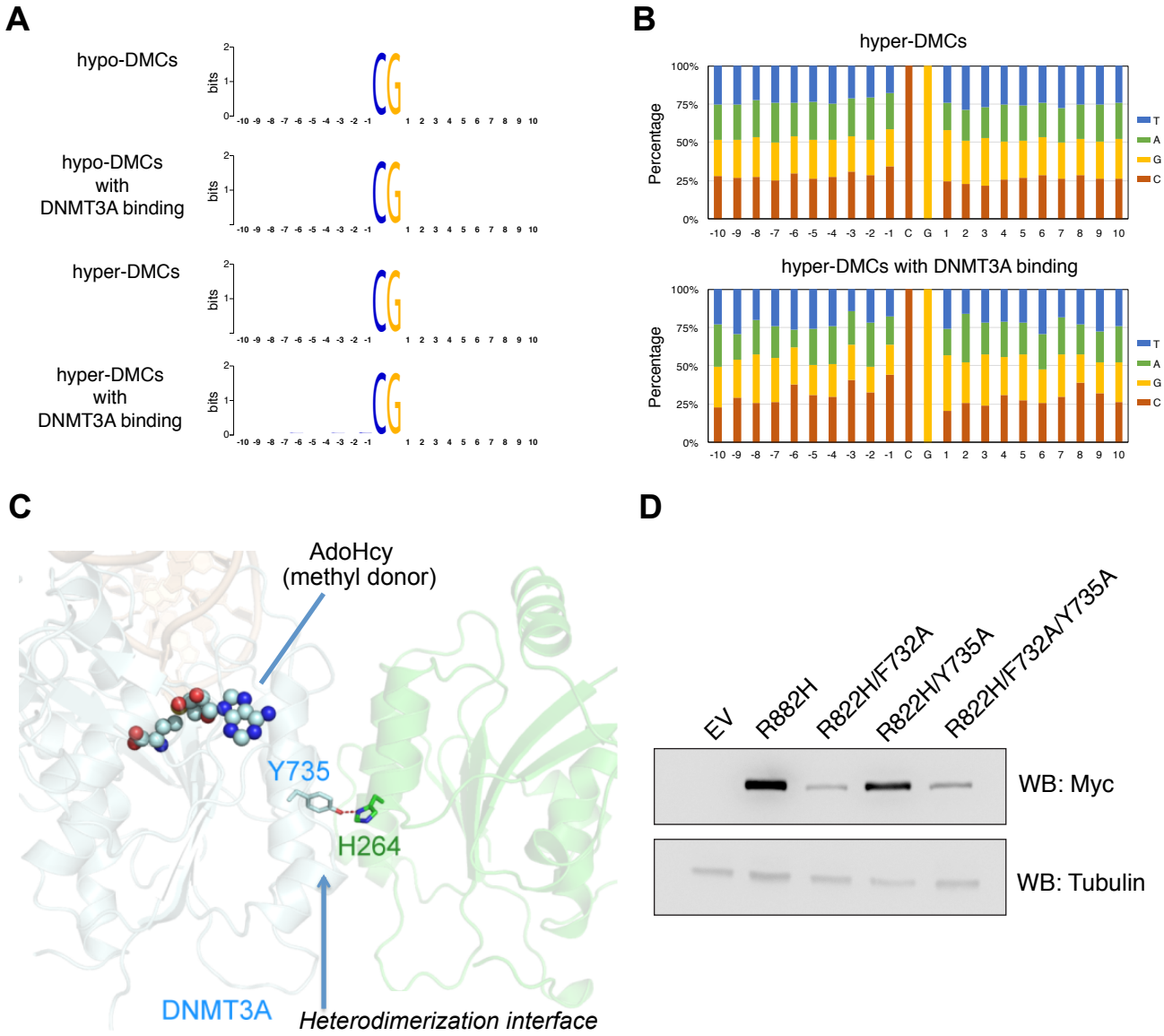

Supplemental Figure 5

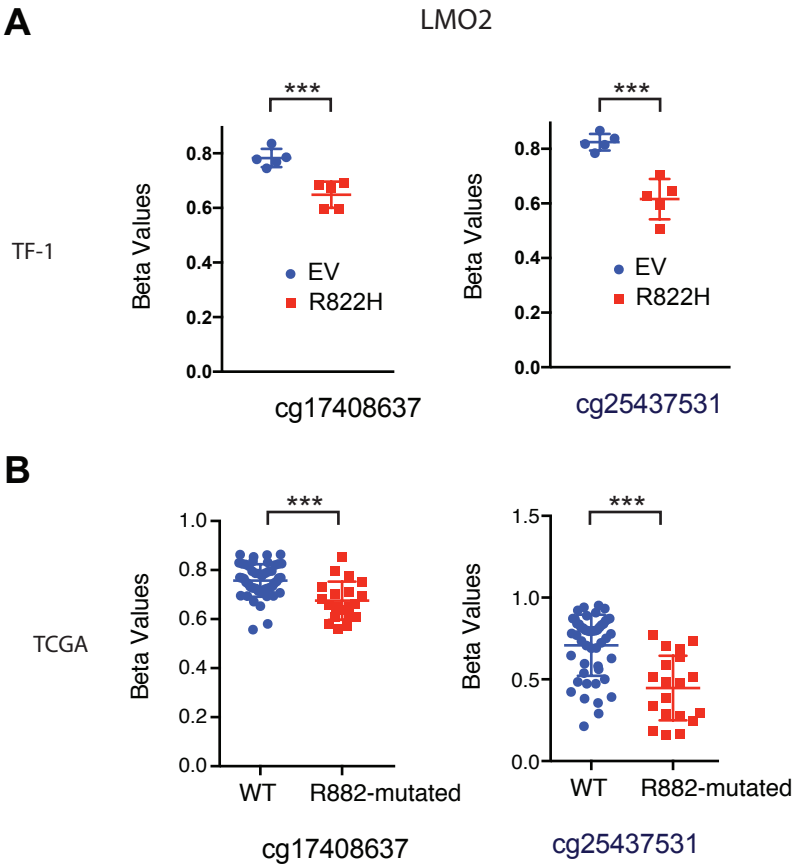

Supplemental Figure 6

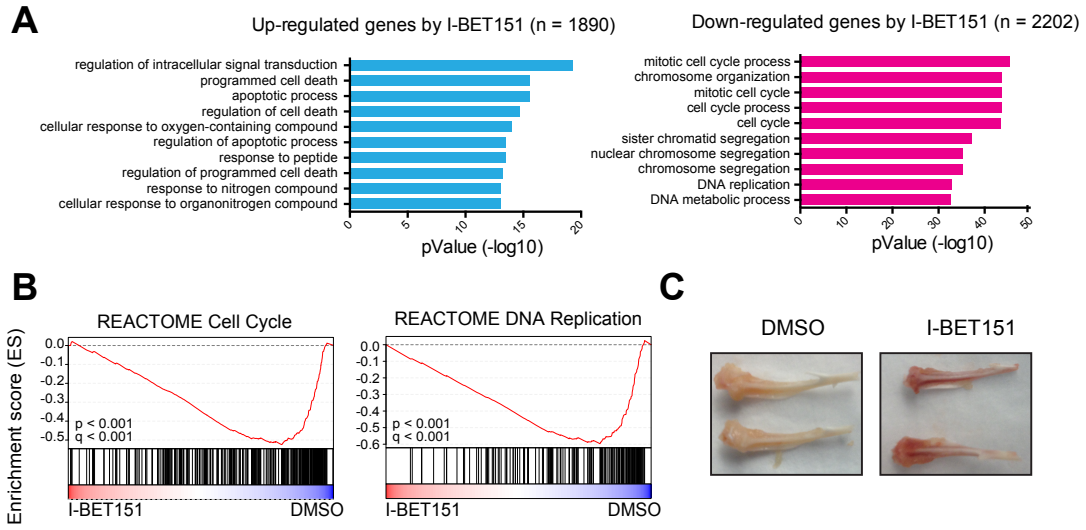

Supplementary Materials and Methods and Tables

Plasmids

Myc-tagged human DNMT3A isoform 1 (DNMT3A1) was cloned into MSCV-puro retroviral vector (Clontech) and LeGO-iG2 lentiviral vector (Addgene #27341). Mammalian expression plasmids pBabe-puro-Flag-IDH1(R132H), Flag-tagged DNMT3A/DNMT3B (1) and MSCV-Luciferase were kindly provided by Drs. Y Xiong, T Chen and Q Zhang, respectively. DNMT3A mutation was generated by QuikChange II XL Site-Directed Mutagenesis Kit (Agilent). Lentiviral pLKO.1 human DNMT3A shRNA vectors (TRCN0000035757 and TRCN0000035758) were purchased from Sigma. All plasmid sequences were verified by sequencing.

Cell culture, stable cell line generation, and cell treatment

The cytokine-independent growth of TF1 cells was examined by counting numbers of viable cells by trypan blue exclusion assay post-removal of GM-CSF. To induce erythroid differentiation, TF1 cells were cultured in the RPMI 1640 medium with GM-CSF replaced by 2 ng/ml of human recombinant human erythropoietin (EPO) as described before (2). The previously established murine leukemia cell lines carrying dual DNMT3A^{R882H} and N-RAS mutation were cultured and maintained as described before (3).

To generate TF-1 cell lines stably expressing DNMT3A, IDH1, or their variants, the MSCV-based retrovirus was packaged in HEK293FT cells and used for infection as previously described (2,4). To generate TF-1 cell lines with stable knockdown of DNMT3A, the pLKO-based lentivirus was packaged in HEK293FT cells and used for infection. 48 hrs post infection, TF-1 cells were selected by 2 μg/ml of puromycin for four days and maintained in medium with 0.5 μg/ml of puromycin before use. Treatment with

the BRD4 inhibitor I-BET151 (GSK1210151A; Selleck chemical LLC) was carried out as described (5-7).

Immunoblotting.

Antibodies used for immunoblotting include those for MYC-tag (1:3,000 dilution, Sigma, M4439), Flag tag (1:1,000 dilution, Sigma, M2-HRP, A8592), DNMT3A (1:1,000 dilution, Santa Cruz, H-295), DNMT3B (1:1,000 dilution, Santa Cruz, G-9, sc-376043), and Tubulin (1:3,000 dilution, Sigma, T6199). Cells were washed with cold PBS three times and directly suspended in 2x Laemmli sample buffer (4% SDS, 10% Glycerol, 60 mM Tris-Cl pH 6.8, 5% β-mercaptoethanol, and 0.01% bromophenol blue) in a concentration of 10 million per mL. After boiling and brief sonication, whole cell lysates were subject to SDS-PAGE and western blotting as described before (3).

Flow cytometry analysis

Cells were washed with PBS and incubated with fluorochrome-conjugated antibodies for 30 minutes at 4°C. The antibodies used were PE-Cy5-conjugated mouse anti-human CD235a antibody (1:100, BD Pharmingen, 559944) and R-PE-conjugated Fetal Hemoglobin antibody (1:100, Invitrogen, HFH04). The flow cytometry data were acquired from CyAn ADP cytometer (Beckman Coulter) and analyzed with FlowJo software.

Real-time qPCR (RT-qPCR) analysis

Total RNA was isolated using the RNeasy Mini Kit (Qiagen). First strand cDNA was synthesized using the High-Capacity cDNA Reverse Transcription Kit (Applied Biosystems). Real-time PCR was performed in triplicate using the iTaq universal SYBR Green supermix (Bio-Rad) and the QuantStudio 6 Flex Real-Time PCR System (Applied Biosystems). All values were normalized to GAPDH levels. The primers used for RT-

qPCR analysis were: for GAPDH, 5'- AAC ATC ATC CCT GCC TCT ACT GG-3' and 5'-GTT TTT CTA GAC GGC AGG TCA GG-3'; for DNMT3A, 5'-TAT TGA TGA GCG CAC AAG AGA GC-3' and 5'-GGG TGT TCC AGG GTA ACA TTG AG-3'; for LMO2, 5'-AAGGAACAGGTGCAAAGCAG-3' and 5'-AGCTACTGCAAGTTCAGGTTGA-3'.

Microarray and data analysis

Total RNA was isolated from cell pellets using the RNeasy Plus Mini Kit (Qiagen). Extracted RNA was assessed with Bioanalyzer and subjected to microarray sample preparation and hybridization to Mouse_Gene_2.0_ST arrays (Affymetrix) according to manufacturer's instruction by UNC Functional Genomics Core. Data analysis was performed as described before (8). Briefly, gene expression data were extracted from raw CEL files from the Mouse Gene 2.0 ST arrays by GeneSpring software X12.6 (Agilent Technologies, Inc.). Genes with at least 1.5-fold change and $p < 0.05$ with standard two sample t-test were subjected gene ontology analysis using DAVID Functional Annotation Bioinformatics Microarray Analysis tool (https://david.ncifcrf.gov/). GSEA analysis was performed using GSEA2-2.2.0 software (Subramanian et al., 2005) for testing enrichment of curated gene sets (C2) or customized gene sets.

ChIP-Seq data analysis

ChIP sequencing library was constructed by UNC High-throughput Sequencing Facility and single-end sequenced for 50 bp on an Illumina HiSeq-2500 Sequencer. ChIP-seq data of H3K27ac in murine leukemia cell lines with dual DNMT3A^{R882H} and N-RAS mutations were obtained from the recent published work (3). ChIP-seq reads were mapped to mm9 genome using Bowtie with default parameters. After removing PCR

duplicates using Samtools, peaks were called and bedgraph signal track files were generated using MACS2 software. The track files were viewed using IGV software.

Murine leukemia model and in vivo dosing studies

All animal experiments were reviewed and approved by the Institutional Animal Care and Use Committee of UNC. Briefly, 8-10-week old female Balb/c mice (Jackson Laboratory; cat#: 000651) were subject to sub-lethal irradiation and intravenous injection of murine leukemia lines carrying DNMT3A^{R882H} and RAS mutation as described before (3). For single-agent treatment with I-BET151, mice were inoculated with 0.1 million of murine leukemia cells, randomized into groups and, 5 days post-inoculation, subject to treatment with vehicle only (0.5% methycellulose) or I-BET151 intraperitoneally (50 mg/kg body weight) for five days a week. For combinational treatment, recipients inoculated with 0.1 million of the luciferase-labeled murine leukemic cells per mouse were randomized to different cohorts, followed by treatment with vehicle only, 1 mg/kg of Trametinib (MedChemExpress, Cat#: HY-10999), 50 mg/kg of I-BET151, or their combination through oral gavage for 2 consecutive weeks. Leukemia burdens of each recipient were monitored weekly through in vivo imaging after intraperitoneal injection of 150 mg/kg luciferin (Gold bio, cat#: 115114-35-9; carried out at UNC Animal Studies Core). The phenotypic examination of murine leukemia including pathological and histological analysis was performed as described before (3,8-11).

Statistics

Data are presented as the mean ± SD of at least three independent experiments. Statistical analysis was performed with Student's t test for comparing two sets of data

with assumed normal distribution, and with the Log-rank (Mantel-Cox) test for non-parametric analysis such as Kaplan-Meier survival curve.

Supplementary Figure Legends

Supplementary Figure 1. DNMT3A^{R882}, but not DNMT3A^{WT}, promotes TF-1 cell transformation characterized by the cytokine-independent growth and differentiation arrest.

(A) Domain structure of DNMT3A. A black line indicates R882 mutation.

(B) RT-qPCR analyses of DNMT3A in TF-1 stable cell lines expressing empty vector (EV), DNMT3A^{WT} or DNMT3A^{R882H}.

(C-D) Flow cytometry analysis detects erythroid differentiation, as measured by Glycophorin A (C) or Fetal hemoglobin (D) staining of TF1 cell lines expressing either empty vector (EV), DNMT3A^{WT} (WT) or DNMT3A^{R882H} (R882H) 10 days post-treatment with 2 unit/mL Erythropoietin (EPO).

(E) RT-qPCR analysis of endogenous DNMT3A expression in TF-1 stable cell lines expressing shRNA vector control or either of two independent shRNAs targeting DNMT3A.

(F) Flow cytometry showing EGFP expressing levels in the parental or DNMT3A^{R882H}-transduced TF-1 cell lines, followed by Cre expression to deplete the DNMT3A^{R882H}-IRES-EGFP transgenes (for details, see also Fig 1F, upper panel, for the used LEGO-iG2 vector).

Supplementary Figure 2. DNMT3A^{R882mut} promotes DNA hypo-methylation in TF-1 cells.

(A) Heatmap shows CpG methylation levels of the DNMT3A^{R882H}-associated hypomethylated DMPs in TF-1 stable cell lines expressing DNMT3A^{WT}, relative to vector controls (EV).

(B) Heatmap shows CpG methylation levels of the DNMT3A^{R882H}-associated hypomethylated DMPs in TF-1 stable cell lines expressing DNMT3A^{R882C} (RC) or DNMT3A^{R882S} (RS), relative to EV.

(C) Principal component analysis (PCA) of the indicated human AML samples and TF1 cell lines, based on the methylation levels of the DNMT3A^{R882H}-associated hypomethylated DMPs as detected in TF-1 cells. 450K-array methylome data of human AML samples were from a previous study (12). R882 and non-R882 denote the AML patients carrying a DNMT3A mutation at Arg882 and the site other than Arg882, respectively. n, cohort size.

Supplemental Figure 3. DNMT3A^{R882H} promotes leukemic cell transformation and DNA hypo-methylation in a dose-dependent manner.

(A) Representation of flow cytometry analysis and the gates for sorting cells with different levels of EGFP expression. L: low; M: medium; H: high; VH: very high. Upper panel shows a schematic representation of the LeGO-G2 lentiviral vector that contains a DNMT3A-IRES-EGFP cassette. SIN-LTR: self-Inactivating long terminal repeat; RRE: rev response element; cPPT: central polypurine tract; spleen focus-forming virus promoter; IRES: internal ribosome entry site; wPRE: woodchuck hepatitis posttranscriptional regulatory element.

(B). Methylation levels shown in beta values (y-axis) as detected by the 450K-array platform at the indicated genes in TF-1 stable cell lines expressing different doses of DNMT3A^{R882H}, relative to control. L: low; M: medium; H: high.

Supplemental Figure 4. Features of the DNMT3A^{R882H}-associated, differentially methylated CpG sites (DMCs).

(A) Motif analysis of sequences (-10 to +10 base pairs) surrounding the indicated DMCs based on eRRBS DNA methylation profiling of hematopoietic stem and progenitor cells (HSPCs) with enforced expression of DNMT3A^{R882H} as done in a recent work (3). Hypo- or hyper-DMCs were CpG sites showing the DNMT3A^{R882H}-induced loss (hypo) or gain (hyper) of DNA methylation, respectively. DMCs with DNMT3A binding were those showing the direct DNMT3A^{R882H} binding based on ChIP-seq data (3).

(B) Distribution of nucleotide sequences surrounding the DNMT3A^{R882H}-induced hyper-methylated CpG sites, either with (bottom) or without (top) direct binding of DNMT3A^{R882H}.

(C) The heterodimerization interface of DNMT3A complexes that contains Y735, based on to published works (2,13).

(D) Immunoblotting of Myc-tagged DNMT3A after stable transduction into TF-1 cells.

Supplemental Figure 5. DNA methylation levels of DMPs at the LMO2 gene identified in TF-1 cells (panel A) and human AMLs (B) with DNMT3A^{R882mut}. 450K-array methylome data of human AML samples were obtained from a previous study (12).

Supplemental Figure 6. BRD4 blockade is efficient in treatment of murine AML established by combinational DNMT3A^{R882H} and NRAS^{G12D} mutations.

(A) Gene ontology (GO) analysis of genes up- and down-regulated by I-BET151 in the DNMT3A^{R882H}/NRAS^{G12D} AML cells.

(B) GSEA analysis showing selected the indicated gene signature repressed by I-BET151 relative to DMSO.

(C) Images of bones from leukemic mice treated with vehicle and I-BET151, which displayed pale and pink in color, respectively.

Supplemental Table 1. List of the differentially methylated CpG probes (DMPs) induced by DNMT3A^{R882H} in TF-1 cells.

Reference:

1. Kim SJ, Zhao H, Hardikar S, Singh AK, Goodell MA, Chen T. A DNMT3A mutation common in AML exhibits dominant-negative effects in murine ES cells. Blood 2013;122(25):4086-9.
2. Zhang ZM, Lu R, Wang P, Yu Y, Chen D, Gao L, et al. Structural basis for DNMT3A-mediated de novo DNA methylation. Nature 2018;554(7692):387-91.
3. Lu R, Wang P, Parton T, Zhou Y, Chrysovergis K, Rockowitz S, et al. Epigenetic Perturbations by Arg882-Mutated DNMT3A Potentiate Aberrant Stem Cell Gene-Expression Program and Acute Leukemia Development. Cancer cell 2016;30(1):92-107.
4. Wang GG, Calvo KR, Pasillas MP, Sykes DB, Hacker H, Kamps MP. Quantitative production of macrophages or neutrophils ex vivo using conditional Hoxb8. Nature methods 2006;3(4):287-93.
5. Cai L, Tsai YH, Wang P, Wang J, Li D, Fan H, et al. ZFX Mediates Non-canonical Oncogenic Functions of the Androgen Receptor Splice Variant 7 in Castrate-Resistant Prostate Cancer. Molecular cell 2018.
6. Zuber J, Shi J, Wang E, Rappaport AR, Herrmann H, Sison EA, et al. RNAi screen identifies Brd4 as a therapeutic target in acute myeloid leukaemia. Nature 2011;478(7370):524-8.
7. Dawson MA, Prinjha RK, Dittmann A, Giotopoulos G, Bantscheff M, Chan WI, et al. Inhibition of BET recruitment to chromatin as an effective treatment for MLL-fusion leukaemia. Nature 2011;478(7370):529-33.
8. Xu B, On DM, Ma A, Parton T, Konze KD, Pattenden SG, et al. Selective inhibition of EZH2 and EZH1 enzymatic activity by a small molecule suppresses MLL-rearranged leukemia. Blood 2015;125(2):346-57.
9. Wang GG, Song J, Wang Z, Dormann HL, Casadio F, Li H, et al. Haematopoietic malignancies caused by dysregulation of a chromatin-binding PHD finger. Nature 2009;459(7248):847-51.
10. Wang GG, Cai L, Pasillas MP, Kamps MP. NUP98-NSD1 links H3K36 methylation to Hox-A gene activation and leukaemogenesis. Nature cell biology 2007;9(7):804-12.
11. Wang GG, Pasillas MP, Kamps MP. Meis1 programs transcription of FLT3 and cancer stem cell character, using a mechanism that requires interaction with Pbx and a novel function of the Meis1 C-terminus. Blood 2005;106(1):254-64.
12. Russler-Germain DA, Spencer DH, Young MA, Lamprecht TL, Miller CA, Fulton R, et al. The R882H DNMT3A mutation associated with AML dominantly inhibits wild-type DNMT3A by blocking its ability to form active tetramers. Cancer cell 2014;25(4):442-54.
13. Jia D, Jurkowska RZ, Zhang X, Jeltsch A, Cheng X. Structure of Dnmt3a bound to Dnmt3L suggests a model for de novo DNA methylation. Nature 2007;449(7159):248-51.